University of Alberta

Adsorptive Air Separation Behaviour on Silver Exchanged ETS–10 Typed Molecular Sieves

by

Somayeh Sarabadan

A thesis submitted to the Faculty of Graduate Studies and Research In partial fulfillment of the requirement for the degree of:

Master of Science

in

Chemical Engineering

Department of Chemical and Materials Engineering

This thesis is lovingly dedicated:

To my mother, Kobra
For her sacrifice, devotion, never ending love and constant prayers

To my father, Reza
For his love and encouragement in pursuits of my passions

To my beloved husband, Ali
Who always gives me measureless love and support

Abstract

Air Separation is the largest industrial separation process in the world in which air is separated to its primary constituents including, nitrogen, oxygen, and argon. Technical gases are applied in many important industries such as steel industry, chemical processes, oil and gas production, refinery, glass industry, food industry, Electronics and instrument making, and medical applications.

Several different silver-exchanged ETS-10 adsorbents were developed. Sorption of nitrogen, oxygen, and argon on adsorbents were studied by performing inverse gas chromatographic and adsorption isotherm measurements. Isotherms data for nitrogen, oxygen, and argon were fitted by Langmuir model very well and values for adsorption capacities and Henry's selectivities were calculated at 298 K. The proposed data suggests that silver–exchanged ETS-10 exhibits extraordinary behaviour towards adsorption of nitrogen and argon. It is believed that exploiting a single step PSA unit, Ag-ETS-10 is a strong candidate to produce pure nitrogen and high purity oxygen from air.

Acknowledgments

This is a great opportunity to express the appreciation to many people who assisted me in the completion of my research directly and indirectly. I appreciate careful guidance and precious advice received from my supervisor, Dr. Steven Kuznicki. Without his generous support, friendly supervision, and encouragement this work would have never been completed.

Dr. Maham provided all kinds of support and consultation for me during the course of this work. I am grateful to him for his invaluable comments and all the help he provided.

I sincerely thank Lan Wu, Tong Qiu, Adolfo Avila, Weizhu An, and every member of our research group for their general contributions and perspectives. Special thanks to Dr. Tetyana Kuznicki, Dr. Amy Dambrowtiz, Albana Zeko for their assistance. My special thanks to Lily Laser, Graduate Administrative Assistant, for her kind and invaluable help and supports during these years.

I owe my utmost gratitude to my dear friend and colleague, Farnaz for her support, constructive suggestions and discussions. She constantly supported me through the process of completing this thesis with her generous friendship.

I also would like to thank my wonderful supportive friends Sabereh, Rosa, Carolina S., Carolina F. Mariangel, Naeimeh, Rojin, Arezoo, Roya, Nilufar, Maryam, Samira, Mahyar, Somayeh, Niousha, Lina, Fatemeh, Parastoo, Marjan and all other friends whom I am honoured of their friendship. I never forget the joyful and happy moments I had in their company.

I cannot find words to express my gratitude to my lovely husband, Ali whose inspiration, tireless love, constant support and great mentorship make me feel I can do anything. I thank God every moment that you are in my life. Without you, these accomplishments would mean nothing. I LOVE YOU!

I am indebted to my dear parents who have been the greatest supporters throughout my life. I would like to deeply thank them for all the love, sacrifice, unconditional support, invaluable advice, inspiration, and for all other reasons beyond measure. I am really proud of having such wonderful parents. You have inspired me to become the person I am today and I will never forget values you've taught me!

I am also grateful to my wonderful siblings, Samaneh and Mohemmed for their sacrifice and kind support all through my studies and life.

Table of Contents

List of Tables

List of Figures

Nomenclature

Symbol	Description
BEA	Beta Zeolite
BET	Brunauer, Emmett, Teller
CEC	Cation exchange capacity
CMS	Carbon molecular sieve
EDX	Energhy dispersive X-ray
ETS-4	Engelhard titanosilicate number 4
ETS-10	Engelhard titanosilicate number 10
$\widetilde{H}_g$	Molar enthalpy of gaseous adsorbent
$\bar{H}_1$	Partial molar enthalpy of gaseous adsorbent
IAST	Ideal adsorbed solution theory
IGC	Inverse gas chromatography
LSX	Low silica X
OD	Outer diameter
PSA	Pressure swing adsorption
psi	Pound per square inch
PVDC	Poly vinylidene chloride
SEM	Scanning electron microscopy
STP	Standard temperature and pressure
TCD	Thermal conductivity detector
TSA	Temperature swing adsorption
VPSA	Vacuum pressure swing adsorption
VSA	Vacuum swing adsorption
XRD	X-ray powder diffraction
ZSM-5	Zeolite socony mobil-5

Greek letters

Symbol	Description
α	Adsorption rate constant/ Limiting selectivity/ Polarizability
β	Desorption rate constant
γ	Activity coefficient
υ	The amount of gas adsorbed on the adsorbent at equilibrium
ΔG	Free energy change
ΔH	Enthalpy change

ΔS	Entropy change
δH_{iso}	Isosteric heat of adsorption
$\Delta \bar{H}_1$	Differential heat of adsorption
ε	Monolayer volume of the adsorbent/ Potential field
θ	Fractional surface coverage/ Diffraction angle
θ_T	Total surface coverage
μ	Permanent dipole moment/ Chemical potential
π	Spreading pressure/ Pi (constant)
χ	Magnetic susceptibility
σ	Condensation (adsorption) coefficient/ Effective kinetic diameter/ Interfacial tension of the monolayer covered surface
σ^0	Interfacial tension of the clean surface
ϕ	Interaction energy/ Potential function
ϕ_D	Dispersion energy
ϕ_F	Field-dipole interaction energy
ϕ_{FQ}	Field-quadrupole interaction energy
ϕ_P	Polarization energy
ϕ_R	Close-range repulsion energy
φ	Potential energy

Notations

^{o}	Degree
A	Pre-exponential factor/ Surface area
$Å$	Angstrom
B	Empirical constant for the Lennard-Jones 6-12 potential/ Langmuir adsorption constant
b	Toth equation parameter
C	Dispersion constant
c	BET constant/ Speed of light
D	Diffusivity
D/r^2	Rate constant
E	Constant pair interaction energy
E_a	Adsorption activation energy
E_d	Desorption activation energy
F	Field gradient/ Field strength
G	Gibbs free energy

g_m	Molar Gibbs free energy
i	Component
K	Henry's law constant/ Kelvin temperature unit
k	Boltzmann constant/ Freundlich adsorption constant
K_L	Langmuir equation parameter
L	Liquefaction
M	Molar concentration
m	Mass
meq	Milliequivalent
n	Adsorbate concentration/ Number of moles
n_m	Monolayer capacity
n_T	Total number of moles of the adsorbed mixture
P_o	Saturation pressure
P_i	Partial pressure of i
P_i^0	Equilibrium vapor pressure of pure component i
P_s	Saturation pressure
Q	Heat of adsorption for physically adsorbed species/ Quadrupole moment
q	Quantity of gas adsorbed
q_m	Maximum amount adsorbed
R	Gas constant
r	Rate of condensation/ Separation distance
r_{min}	Minimum separation distance
S	Entropy/ Selectivity
S_{ext}	External surface
S_{int}	Internal surface
S_{total}	Equivalent specific surface
T	Temperature
t	Toth equation parameter
V	Volume
v	Adsorbed concentration (volumetric basis)
v_m	Monolayer capacity (volumetric basis)
X_i, x_i	Composition of i in the adsorbed phase
Y_i, y_i	Composition of I in the gas phase

Chapter 1

Introduction

1.1 Air Separation

Air separation is one of the most important gas separation processes in the world in which atmospheric air is separated to its primary constituents. High purity oxygen production is essential in medical applications and enriched oxygen (95% pure) is used in steel, pulp, paper, and glass industries. To yield oxygen with very high purity, argon must be removed from oxygen in a mixture of 95% oxygen balanced with argon. This is challenging because of the similar physical properties (kinetic diameters and boiling points) of oxygen and argon.

There are mainly two basic technologies to separate air, including: cryogenic air separation and non-cryogenic air separation. The basic technological choice between these two mentioned methods is largely determined by [1]:

- The number of the products that must be supplied (e.g., nitrogen, oxygen, or argon or all)

- The required production rates for each gas product

- Required product purities

While cryogenic systems work at very low temperatures, non-cryogenic systems operate at near ambient temperatures. Non-cryogenic processes can be further divided into adsorptive processes such as pressure swing and vacuum swing adsorption, and membrane separation processes.

1.1.1 Air Separation by Cryogenic Distillation

Cryogenic distillation is a traditional method for air separation initiated by Carl von Linde in the early 20th century and is based on the differences in the relative volatilities of the components. This method is used to produce highly purified gases or liquids products at very low distillation temperatures. A large volume of atmospheric air is separated through three consecutive stages: compression, purification, and distillation. Impurities must be removed in the compression step. In the cryogenic distillation process, the equipment used such as distillation columns, piping connections, and heat exchangers are kept at very low temperatures in well-insulated cold boxes [1, 2]. There are variations in the cryogenic air separation cycles depending upon:

- The number of the required products from the cycle (whether simply oxygen or nitrogen, or both oxygen and nitrogen, or nitrogen, oxygen, and argon).

- The maximum allowed product impurity.

- The required delivery pressures of the gaseous products.

- The state at which products (liquid of gas) should be stored.

Although this traditional method is simple, and produces high purity products, it is only cost effective for medium to large scale plants and has a high-energy requirement. [3, 4]

1.1.2 Air Separation via Non-Cryogenic Methods

Non-cryogenic techniques were developed during the 1970s. Non-cryogenic processes exploit differences in the physical properties of the compounds, such as

molecular structure, size and mass to generate oxygen or nitrogen and operate at near ambient temperatures. Unlike the cryogenic method, these techniques are efficient at a low energy cost with the capability of regenerating the adsorbent several times. But they are best suited for small production rates of oxygen and nitrogen of lower purity. This is because the physical size of the plant can be decreased as required purity is reduced, and the power needed to operate the unit is reduced as well [3, 4]. In addition, non-cryogenic plants are relatively easy to set up, which is useful when full-time production is not needed. The most commonly used non-cryogenic methods are adsorptive separation processes and membrane separation processes.

1.1.2.1 Air Separation by Membranes

Membrane air separation is based on the differences in diffusion rates of different gases in the mixture through a membrane. Oxygen in the dry air diffuses much faster through the tube walls than argon and nitrogen, and the difference in the diffusion rates allows dry air to be separated into a product which is a mixture of mostly nitrogen and argon, and a low-pressure permeate enriched in oxygen. Majority of membrane materials are more permeable to oxygen than nitrogen and argon due to smaller size of the oxygen molecule [1, 5]. Flux and selectivity are two important properties that determine the economics of the membrane processes. Flux determines the membrane surface area and is a function of the pressure difference divided by the membrane thickness. A constant of proportionality that varies with the type of membrane is called the permeability. Membrane selectivity is defined as the ratio of the permeabilities of the gases to be separated. The main advantages of the membrane separation that make it attractive for larger oxygen requirements, are its simplicity, continuous nature of the process, and working near ambient temperature and pressure that also allow for quick start-up operations [5, 6]

A recently developed membrane separation technology for large oxygen production is the Ion Transport Membrane (ITM). ITMs are solid inorganic oxide

ceramic materials that separate oxygen as it passes through the ceramic crystal structure. At the surface of the membranes, oxygen molecules are converted to the oxygen ions and then these ions are transferred through the membrane at very high flow rates by an applied electric voltage or oxygen partial pressure difference. Oxygen molecules are then reformed again after passing through the membrane material. This technology is a fundamentally different approach for production of high quality and high volume oxygen at a lower cost [5].

1.1.2.2 Air Separation by Adsorption

Adsorption separation processes are based on the ability of some natural and synthetic molecular sieves to selectively adsorb one of the components in the gaseous mixture. Adsorptive separations such as pressure swing adsorption (PSA) and vacuum pressure swing adsorption (VPSA) processes rely upon the fact that under pressure, gases tend to be adsorbed to the adsorbent surface. The higher the pressure, the more gas is adsorbed but once the pressure is dropped, the gas is released and desorption happens [6-8].

Zeolite molecular sieves are typically used in adsorption-based processes for oxygen production. They have non-uniform electrostatic fields in their zeolitic voids which result in preferential adsorption of the molecules with higher polarizability or higher quadrupole moments. Nitrogen has a bigger quadrupole moment and consequently a stronger interaction with adsorbate cationic sites, allowing nitrogen molecules to adsorb stronger than oxygen and argon. In air separation, as air passes through the zeolitic bed, nitrogen is retained and enriched oxygen is produced in the up-stream [2, 5, 9-12].

On the other hand, carbon molecular sieves have pore apertures on the same order of magnitude as the size of components of air. Since the kinetic diameter of the oxygen molecules is slightly smaller than that of nitrogen molecules, they diffuse more rapidly into the pores of the adsorbent. Thus, carbon molecular sieves are more selective for oxygen while zeolites are more selective for nitrogen. [2, 13-17].

1.2 Adsorption

All adsorption separation processes involve two major steps: adsorption and desorption. During adsorption, preferentially adsorbed gaseous (liquid) adsorbate molecules accumulate on the solid adsorbent surface. Adsorption is different from absorption, in which a substance diffuses into liquid or solid to form a solution. Similar to surface tension, adsorption is a consequence of surface energy. Desorption or regeneration is the phenomenon of removing the substances from the adsorbent surface and thus regenerating the adsorbent for use in the next adsorption cycle. The species that is released during the desorption step contains the more strongly adsorbed species in concentrated form (compared to the feed) and is sometimes called the extract product.

As in all adsorption separation processes, the essential requirement is an adsorbent that preferentially adsorbs one component from a mixed feed. To measure this characteristic of the adsorption, the selectivity parameter is used. Selectivity depends on either a difference in adsorption equilibrium or on a difference in adsorption rates (kinetic selectivity). In certain cases the differences in rates may be so great that the slower-diffusing species is in effect totally excluded from the adsorbent (size-selective sieving) resulting in a very efficient separation. Selecting the appropriate adsorbent is the key factor to obtain a good separation which is discussed in the next section.

1.3 Adsorbent Selection

The most important requirement of any economic adsorption process is finding an adsorbent with sufficient selectivity, capacity, kinetics, and regenerability. High selectivity and capacity (which is measured using adsorption isotherms) result in high productivity. To have a feasible separation while avoiding large costly equipment, the adsorbent must have a reasonably high capacity. Capacity depends on the adsorbent surface area. Therefore, the higher the surface area the higher the capacity is. An efficient adsorbent however needs to have both high capacity and optimal kinetics capable of transferring adsorbing molecules quickly

to the adsorption sites [6, 7, 18, 19]. All cyclic adsorption applications rely on regenerability, so that the adsorbent can operate in sequential cycles with uniform performance. The regenerability of an adsorbent influences the fraction of the original capacity that is retained, and the required time, and energy for regeneration. Various practical adsorbents including activated carbon, zeolite, alumina and silica gel are employed in different industries such as chemical, petrochemical, biochemical, biological and biomedical. Some of the commercial adsorption processes with different adsorbents are listed in the table (1.1) [7, 8].

Table 1.1 Examples of commercial adsorption processes and applied adsorbents

Separation	Adsorbent
Gas Bulk Separations	
Normal paraffins/isoparaffins, aromatics	Zeolite
N_2/O_2	Zeolite
O_2/N_2	Carbon molecular sieve
CO, CH_4, CO_2, N_2, Ar, NH_3/H_2	Activated carbon followed by zeolite
Hydrocarbons/vent streams	Activated carbon
H_2O/ethanol	Zeolite (3A)
Chromatographic analytical separations	Wide range of inorganic and polymer resin agents
Gas Purification	
H_2O/olefin-containing cracked gas, natural gas, air, synthetic gas, etc.	Silica, alumina, zeolite (3A)
CO_2/C_2H_4, natural gas, etc.	Zeolite, carbon molecular sieve
Hydrocarbons, halogenated organics, solvents/vent streams	Activated carbon, silicalite, others
Sulfur compounds/natural gas, hydrogen, liquefied petroleum gas (LPG), etc.	Zeolite, activated alumina
SO_2/vent streams	Zeolite, activated carbon
Odors/air	Silicate, others
Indoor air pollutants- VOCs	Activated carbon, silicate, resins
Tank-vent emissions/air or nitrogen	Activated carbon, silicate
Hg/chlor-alkali cell gas effluent	Zeolite

Activated carbon, activated alumina, and silica gel do not have an ordered crystal structure and consequently the pores are not uniform. The distribution of the pore diameters within the adsorbent particles may be narrow (20 to 50 Å) or it may range widely (20 to several thousand Å) as is the case for some activated carbon molecular sieves. Hence all molecular species with the possible exception of high molecular weight polymeric materials may enter the pores. Zeolite molecular sieves have pores of uniform size (3 Å to 10 Å) which are uniquely

determined by the unit structure of the crystal. These pores will completely exclude molecules which are larger than their diameter.

1.3.1 Zeolites

Zeolites are porous crystalline, hydrated aluminosilicates of alkali and alkali earth elements, such as sodium, potassium, and calcium which may be represented by the following empirical formula [20]:

$$M_{x/n}\left[(AlO_2)_x(SiO_2)_y\right] \cdot wH_2O$$
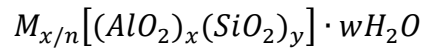
Where, *M* is the cation of valence *n*, *w* is the number of water molecules and the ratio *y/x* usually has values of 1-5 depending upon the structure. The primary structural units of zeolites are the tetrahedral of silicon and aluminum, $[SiO_4]$ and $[AlO_4]$ which are linked together by sharing all of the oxygen resulting in an infinite extending three-dimensional network of $[AlO_4]$ and $[SiO_4]$. The water can be reversibly removed by heating and consequently it will leave a microporous structure which may account for up to 50% of the crystals by volume.

Zeolite frameworks are typically anionic due to one negative charge coming from AlO_4^- while charge compensating cations populate the pores to maintain electrical neutrality. These cations are exchangeable and confer some important properties for zeolites. Varying the position and the type of the cations changes the channel size and the properties of the zeolite, including its selectivity. The zeolitic channels or pores are microscopically small and have molecular sieve dimensions such that they are often named "molecular sieves". The size and the shape of the channels have extraordinary effects on the adsorptive properties of these materials making them useful in separation processes. Molecules can be separated by shape and size related to their possible orientation in the pore, or by the difference in the strength of adsorption. Due to the presence of the zeolitic channels, zeolites have a higher internal surface area available for adsorption, while their external surface contributes only a small amount of the total available surface area.

7

Classical aluminosilicates molecular sieves have pore sizes ranging from 2.5 Å to 10 Å and some of them can only be modified to some extent by cation exchange within the porous framework. For example, Na-A has pore size of about 3.8 Å which can be reduced to 3.3 Å in K-A due to larger potassium cationic size. But this reduction in size is not a gradual change but a sudden change. Therefore, with respect to separation processes zeolites with widely different adsorptive properties may be tailored by the appropriate choice of framework structure, cationic form, and silica to alumina ratio in order to obtain the selectivity required for a given separation. Many zeolites are extremely polar and therefore separations may be affected using both molecular sieving and internal surface property effects. The kinetic selectivity is determined from the free diameters of the windows in the intra-crystalline channel structure. Several examples of such diameters, along with the principal properties and main applications of the zeolites are given in Table (1.2) [7, 18, 20].

Table 1.2 Some major applications of zeolite adsorbents

Framework	Cationic form	Window	Effective channel diameter (nm)	Application
A	Na	8-ring (obstructed)	0.38	Desiccants, CO_2 removal from natural gas
	Ca	8-ring (free)	0.44	Linear paraffin separation, Air separation
	K	8-ring (obstructed)	0.29	Drying of cracked gas containing C2H4
X	Na	12-ring	0.84	Pressure swing H2 purification
	Ca	12-ring	0.80	Removal of mercaptans from natural gas
	Sr, Ba	12-ring	0.80	Xylene separation
	Na	12-ring	0.80	Xylene separation
Y	K	12-ring	0.80	Xylene separation
Mordenite	Ag	12-ring	0.70	I and Kr removal from nuclear off-gases
	H			
ZSM-5	Na	10-ring	0.60	Xylene separation

1.3.2 Carbon Molecular Sieves

Activated carbon adsorbents generally show very little selectivity for molecules of different sizes due to their wide distribution of different pore sizes (20 Å to several thousand Å). However, by special activation procedures it is

possible to prepare carbon adsorbents with a very narrow distribution of micropore sizes that behave as molecular sieves.

Carbon molecular sieves (CMS) are more efficient in the separation processes involving wet gas streams than zeolites, since they are less hydrophilic and still have the molecular sieving properties. There are three methods for preparation of CMS [7]:

1. Carbonization of polymers, such as poly-vinylidene chloride (PVDC)

2. Carbonizing coals slightly, by controlled oxidation and subsequent thermal treatment, especially anthracite or hard coal

3. Coating of the pore mouths of the commercial activated carbon with a carbonized or coked thermosetting polymer

Using one of the three above-mentioned methods, it is possible to make CMS with effective micropore diameter ranging from about 4 Å to 9 Å. The micropore size distribution of such sieves is much narrower than in a typical activated carbon resulting in a lower porosity and small adsorptive capacity. By adjusting the conditions of the manufacturing process, effective pore opening of the CMS can be simply modified to reach the appropriate size for a particular separation. However, it is difficult to reproduce CMS between various batches, and the presence of pore size distribution, even if narrow, means that molecular sieving selectivity of a CMS rarely approaches that of a zeolite sieve. Nevertheless, the kinetic selectivities which may be attained with a well-prepared CMS are significantly high. It has been proposed that the most important large-scale application of CMS is in air separation [21]. Surprisingly, corrosion of the sieve due to oxidation is not a significant problem in the case of CMS. Other potential areas of application include the clean-up of the off-gases from nuclear facilities and the production of pure hydrogen from the gas streams containing small amounts of hydrocarbons.

1.3.3 Mixed Coordination Molecular Sieves

Mixed coordination molecular sieves resemble classical (tetrahedral) zeolite molecular sieves very closely. These materials have:

- Uniform pore sizes

- Cages of nanometer dimensions

- Loaded with charged sites (make them suitable for adsorption, ion exchange, and catalysis)

Mixed coordination molecular sieves contain structural units that are fundamentally different from classical aluminosilicates. They are constructed of chains of octahedral atoms such as titanium, vanadium, zirconium, and niobium interwoven with rings of tetrahedral atoms such as silicon, aluminum, and gallium. ETS molecular sieves such as ETS-4 [22] and ETS-10 [23] are the most known examples where octahedral atoms are titanium and tetrahedral atoms are silicon. Engelhard Titanosilicate-10 (ETS-10) is a three-dimensional 12-membered ring network with pore size of about 0.8 nm and with a Si/Ti ratio of approximately five. The presence of each tetravalent titanium atom in an octahedron generates two negative charges which are balanced with two exchangeable monovalent cations for each structural titanium. ETS-10 is usually synthesized in the sodium form. Owing to its wide-pore nature and thermal stability, ETS-10 is perhaps the most important octahedral/ tetrahedral framework microporous titanosilicate synthesized until to date [24]. The most interesting aspect of ETS-10 structure is that it consists of infinite –O–Ti–O–Ti–O– chains which are surrounded by silicate ring structures. The ETS-10 pore structure has 12-ring in all three-dimensions.

Mixed coordination molecular sieves exhibit some extraordinary characteristics which cannot be seen in any classical zeolite molecular sieves. These amazing properties are explained below [23, 24, 25-28]:

- *Molecular Gate Effect*: This property stands for the systematic pore shrinkage of ETS molecular sieves through dehydration at elevated

temperatures. The ability to tune the effective size of the pores provides access to the interior of the crystal. This effect can be exploited to tailor the adsorption properties of the materials produce size selective adsorbents suitable for commercially important separations of gas mixtures of almost identical sizes (in the 3.0-4.0 Å range) such as N_2/CH_4, Ar/O_2, and N_2/O_2. For instance, ETS-4 pore size can be contracted through calcination from 4.5 Å down to 2.5 Å.

- *Anion Replacement*: The effective pore size of the titanosilicate materials could be controlled by substituting anions that are usually hydroxyl groups (OH^-) and can be replaced with any of halogens. The quantity and type of halogen determines the adsorptive properties of the molecular sieve. Substitution of hydroxyl groups with large halogens such as Cl^- and I^- results in pore reduction. This method of tailoring the effective pore sizes of the titanosilicate molecular sieves has important applications such as in purification of light hydrocarbons and air separation [26].

- *Easy substitution of both octahedral and tetrahedral framework sites*: Both octahedrally coordinated titanium and tetrahedral silicon atoms can be partially or totally substituted by other metals. For instance, titanium can be totally or partially replaced by cobalt, chromium, copper, iron, germanium, magnesium, molybdenum, niobium, nickel, vanadium, and zirconium and so on. There are also many substitutions for silicon such as aluminum, cobalt, chromium, copper, bismuth, arsenic, iron, gallium, germanium, vanadium, zinc, lead, niobium, and nickel, and so on [21, 24, 29].

1.4 Outline of the Thesis

The research presented in this thesis is focused on modifying the adsorptive properties of ETS-10 molecular sieves through ion exchange, and their subsequent application in N_2/O_2 and Ar/O_2 separations. Chapter two provides background information on the fundamental principles of adsorption and adsorptive processes. Chapter three describes how formation of silver chloride

filaments on the surface of ETS-10 molecular sieves affects N_2/O_2 and Ar/O_2 selectivity. Chapter four shows that silver nanoparticles supported on ETS-10 can be used for molecular separation, such as Ar/O_2 and N_2/O_2. It is believed that fully exchanged Ag-ETS-10 can be a very strong candidate for O_2 production from previously enriched oxygen stream containing approximately 95% O_2 and 5% Ar. In chapter five, adsorptive properties of several different single and mixed cationic–exchanged forms of ETS-10 are compared.

References:

[1] Nexant, I., 2010, "Air Separation Technology".

[2] Rege, S. U., and Yang, R. T., 2000, "Kinetic Separation of Oxygen and Argon using Molecular Sieve Carbon", Adsorption, 6(1) pp. 15-22.

[3] Cabau, I. S., October 2005, "Improvement of the Properties of Zeolites for application in the Nitrogen and Oxygen Separation Process and in Acid Catalysis".

[4] Häring, H., February 2008, "industrial gases processing", Wiley-VCH, Weinheim Germany.

[5] Smith, A. R., and Klosek, J., 2001, "A Review of Air Separation Technologies and their Integration with Energy Conversion Processes", Fuel Processing Technology, 70(2) pp. 115-134.

[6] Ruthven, D.M., 1984, "Principles of Adsorption and Adsorption processes", John Wiley & Sons, Inc., Canada.

[7] Yang, R.T., 2003, "Adsorbents : fundamentals and applications", Wiley-Interscience.

[8] Ralph T. Yang, 1987, "gas separation by adsroption processes", Butterworth, Boston.

[9] Moon, I., Lee, D.,II, Yang, J., 1986, "Air Separation by Adsorption on Molecular Sieve 5A", Korean Journal of Chemical Engineering, 3(1) pp. 15-21.

[10] Rege, S. U., and Yang, R. T., 1997, "Limits for Air Separation by Adsorption with LiX Zeolite", Industrial & Engineering Chemistry Research, 36(12) pp. 5358-5365.

[11] Kotsis, L., Argyelan, J., Szolcsanyi, P., 1982, "Application of Natural Zeolites for Air Separation", Reaction Kinetics and Catalysis Letters, 18(1) pp. 149-153.

[12] Sebastian, J., and Jasra, R. V., 2005, "Sorption of Nitrogen, Oxygen, and Argon in Silver-Exchanged Zeolites", Industrial & Engineering Chemistry Research, 44(21) pp. 8014-8024.

[13] Chagger, H. K., Ndaji, F. E., Sykes, M. L., 1995, "Kinetics of Adsorption and Diffusional Characteristics of Carbon Molecular Sieves", Carbon, 33(10) pp. 1405-1411.

[14] Chen, Y. D., Yang, R. T., and Uawithya, P., 1994, "Diffusion of Oxygen, Nitrogen and their Mixtures in Carbon Molecular Sieve", AICHE Journal, 40(4) pp. 577-585.

[15] Jee, J., Kim, M., and Lee, C., 2005, "Pressure Swing Adsorption Processes to Purify Oxygen using a Carbon Molecular Sieve", Chemical Engineering Science, 60(3) pp. 869-882.

[16] Ruthven, D. M., 1992, "Diffusion of Oxygen and Nitrogen in Carbon Molecular Sieve", Chemical Engineering Science, 47(17-18) pp. 4305-4308.

[17] Yi, H. M., Weiruo, S., Maruti, B., 1991, "Adsorption and Diffusion of Nitrogen, Oxygen, Argon, and Methane in Molecular Sieve Carbon at Elevated Pressures", Separations Technology, 1(2) pp. 90-98.

[18] W. J., T., and Barry, C., 1998, "Adsorption Technology and Design", Elsevier Science & Technology Books.

[19] Duong, D.D., 1998, "Adsorption analysis : equilibria and kinetics", Imperial College Press, .

[20] Breck, D.W., 1974, "Zeolite molecular sieves: structure, chemistry, and use", Wiley, New York.

[21] Kuznicki, S. M., and Thrush, K. A., 1993, "Large-Pored Molecular Sieved Containing at Leat One Octahedral Site Comprising Titanium and at Least Silicon as a Tetrahedral Site", (US Patent 5208006) .

[22] Kuznicki, S. M., 1990, "Preparation of Small-Pored Crystalline Titanium Molecular Sieve Zeolites", 07/449032(US Patent 4938939) .

[23] Kuznicki, and S. M., 1991, "Large-Pored Crystalline Titanium Molecular Sieve Zeolites", 07/348,226(US Patent 5011591) .

[24] Rocha, J., and Anderson, M. W., 2000, "Microporous Titanosilicates and Other Novel Mixed Octahedral-Tetrahedral Framework Oxides", European Journal of Inorganic Chemistry, 2000(5) pp. 801-818.

[25] Kuznicki, S. M., Bell, V. A., Nair, S., 2001, "A Titanosilicate Molecular Sieve with Adjustable Pores for Size-Selective Adsorption of Molecules", Nature, 412(6848) pp. 720-724.

[26] Lin, C. C. H., Sawada, J. A., Wu, L., 2009, "Anion-Controlled Pore Size of Titanium Silicate Molecular Sieves", Journal of the American Chemical Society, 131(2) pp. 609-614.

[27] Anson, A., Kuznicki, S. M., Kuznicki, T., 2009, "Separation of Argon and Oxygen by Adsorption on a Titanosilicate Molecular Sieve", Separation Science and Technology, 44(7) pp. 1604-1620.

[28] Anson, A., Lin, C. C. H., Kuznicki, T. M., 2010, "Separation of ethylene/ethane Mixtures by Adsorption on Small-Pored Titanosilicate Molecular Sieves", Chemical Engineering Science, 65(2) pp. 807-811.

[29] Rocha, J., Brandao, P., Lin, Z., 1997, "The First Large-Pore Vanadosilicate Framework Containing Hexacoordinated Vanadium", Angewandte Chemie International Edition in English, 36(1-2) pp. 100-102.

Chapter 2

Fundamental Principles of Adsorption

2.1 Theory of Adsorption

Adsorption as a surface phenomenon stands for a spontaneous process in which gas atoms, molecules, or ions accumulate on the surface of the solid. An adsorbed species is termed as adsorbate while the material on which adsorption happens is the adsorbent. Molecules and atoms of the gas adsorbate depending upon the nature of the existing forces between adsorbate molecules and solid surface can be classified as either physisorption or chemisorption. Chemisorption involves electron transfer between gas and solid surface while physisorption is governed by van der Waals and electrostatic forces which are result of the ionic atoms and polar groups on the surface. Physisorption is a reversible process since the forces of attraction are very weak, generally less than 10-15 kcal/mole and gaseous adsorbate molecules can be easily desorbed by heating or dropping the working pressure [2, 3]. In gas adsorption processes, only physisorption is observed.

2.2 Physical Adsorption Forces

Many research attempts have been made to investigate the forces holding adsorbate molecules to the atoms on the surface of the adsorbent. Although the quantitative calculation is still impossible, the nature of different involved forces is understood. In a simple explanation, adsorption occurs when the interaction potential energy φ is equal to the work done to bring a gas molecule to the adsorbed state. In general, it is assumed that the adsorbed state is at the saturated vapour pressure. Therefore, the sorbent-sorbate interaction potential energy at operating pressure P is:

$$-\varphi = -\Delta G = \int_{P}^{P_0} V dP = RT ln \frac{P_0}{P} \qquad (2\text{-}1)$$

Where, ΔG is the free energy change and P_0 is the saturated vapour pressure. The total potential between the adsorbate molecules and the adsorbent surface is:

$$\varphi_{total} = \varphi_{adsorbate-adsorbate} + \varphi_{adsorbate-adsorbent} \qquad (2\text{-}2)$$

The adsorbent has only a secondary effect on the adsorbate–adsorbate interaction. For this reason, the focus only will be on the second term, adsorbate–adsorbent potential, and it will simply be referred to φ.

Three basic types of interaction contributed to the adsorbate–adsorbent forces are dispersion, electrostatic, and chemical bonds. Chemical bond interaction has been explored for adsorption only recently [3]. Weak chemical bonds, especially the broad type of the bonds involving π electrons or π–complexation, offer promising possibilities for designing new and highly selective adsorbents. For physical adsorption, the adsorbate–adsorbent potential is:

$$\varphi = \varphi_D + \varphi_R + \varphi_{Ind} + \varphi_{F\mu} + \varphi_{\dot{F}Q} \qquad (2\text{-}3)$$

In which, φ_D = dispersion energy; φ_R = close range repulsion energy; φ_{Ind} = induction energy which refers to interaction between electric field and an induce dipole moment; $\varphi_{F\mu}$ = interaction between electric field (F) and a

permanent dipole moment (μ); φ_{FQ} = interaction between gradient field ($\dot{F}$) and a quadrupole with quadrupole moment Q.

The first two contributions ($\varphi_D + \varphi_R$) are independent of adsorbate–adsorbent systems and can operate on all of the systems [3]. The last three terms arise from charges which create electrostatic fields on the solid surface. The dispersive forces which were first identified by London [3, 4] exist between any two atoms or molecules, and in the case of adsorption, it is between adsorbate molecules and atoms on the adsorbent surface. These forces arise from the rapid vibration of electron density in each atom, which induces an electrical moment in the neighbour and consequently creates an attraction between them. These forces are always present in the adsorptive systems between the adsorbate and the adsorbent. The potential energy, φ, between two atoms separated by a distance, r, can be estimated by:

$$\varphi(r) = -Cr^{-6} \tag{2-4}$$

Where, C is one of dispersion constants related to the dipole–dipole interactions. The negative sign in the relation demonstrates attraction.

A theoretical expression was derived for the short range repulsive potential, an exponential function of distance, exp (-kr), which can be approximated by:

$$\varphi(r) = +Br^{-12} \tag{2-5}$$

Therefore, the total potential energy becomes:

$$\varphi(r) = -Cr^{-6} + Br^{-12} \tag{2-6}$$

The ($\varphi_D + \varphi_R$) is known as the London or van der Waals forces. In the case of spherical nonpolar molecules, it is well described by equation (2-6) and familiar as Lennard–Jones potential as illustrated in Figure (2.1) [3]. With an equilibrium distance (r_0) at which point $\varphi_D + \varphi_R = 0$. This distance is taken as the average of the van der Waals radii of the interacting pair.

Once the attractive, dispersion constant, C, is known, B is simply obtained by setting $d\varphi/dr = 0$ at r_0. Therefore, $B = Ar_0^6/2$. Remarkably, at r_0, $\varphi_D = -2\varphi_R$. The most commonly used expression for calculating C is the Kirkwood–Müller formula [3, 5]:

$$C = \frac{6mc^2\alpha_i\alpha_j}{(\alpha_i/\chi_i) + (\alpha_j/\chi_j)} \tag{2-7}$$

Where, m is the mass of the electron, c is the speed of light, χ is the magnetic susceptibility, and i and j stand for the two excited atoms or molecules. Some other commonly used relations for calculating C, are including those derived by London, and Slater and Kirkwood [3].
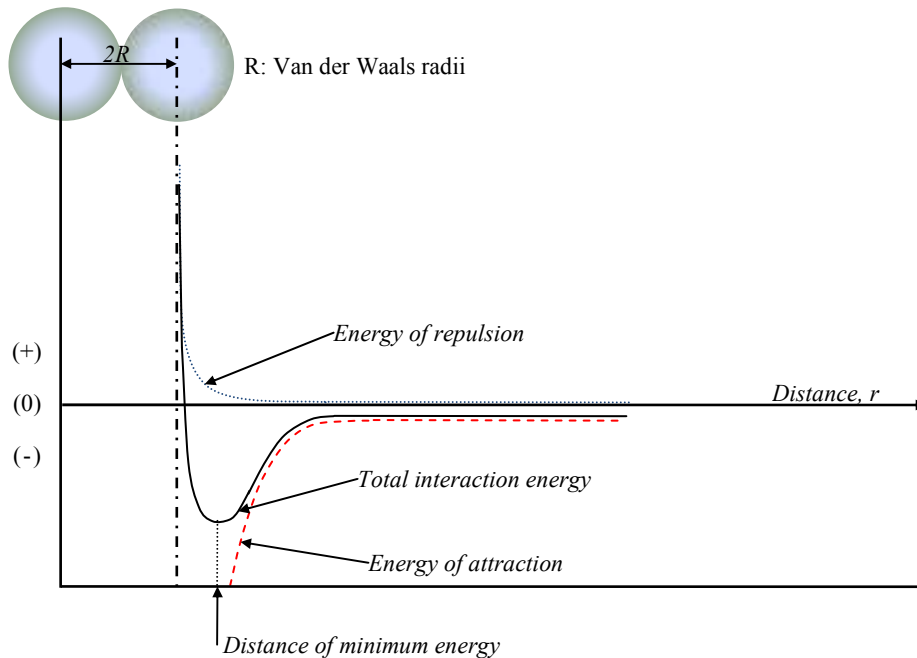
Figure 2.1 The potential energy between two atoms separated by distance r

For a gas molecule and a solid surface separated by distance z, the potential function, $\varphi(z)$, can be calculated by summing all interacting pairs of atoms:

$$\varphi(z) = \varphi_D + \varphi_R = -\sum_i\left(C_{ij}\sum_j r_{ij}^{-6}\right) + \sum_i\left(B_{ij}\sum_j r_{ij}^{-12}\right) \tag{2-8}$$

Interaction energy for a polar surface which induces a dipole moment in the adsorbate molecule is defined as:

$$\varphi_{Ind} = -\frac{1}{2}\alpha^2 F \qquad\qquad (2\text{-}9)$$

Where, F stands for field strength at the center of the adsorbate. If the adsorbate has a permanent dipole moment of μ, and additional energy is with respect to the dipole field interaction:

$$\varphi_{F\mu} = -F\mu\,cos\theta \qquad\qquad (2\text{-}10)$$

In which, θ is the angle between the field and the axis of the dipole moment. For adsorbate molecules processing a quadrupole moment, Q, another term, $\varphi_{\dot{F}Q}$, results from the interaction with the field gradient, $\dot{F}$:

$$\varphi_{\dot{F}Q} = \frac{1}{2}Q\dot{F} \qquad\qquad (2\text{-}11)$$

In considering the forces in adsorption, it is clear that the bond strength should be higher on a surface with higher polarity for a given adsorbate molecule, and for the same surface the bond strength is higher for gas molecules with permanent dipole and quadrupole moments.

2.3 Adsorption Selectivities

One of the common concepts in any kind of separation and gas adsorption is selectivity. Selectivity or separation factor describes the preference of the adsorbent toward competing adsorbates. The selectivity is a function of pressure and temperature. For a given adsorbent, the relative strength of the adsorption of different adsorbate molecules depends upon the relative magnitudes of the polarizability, dipole moment, and quadrupole moment of each species. And for a given adsorbate molecule, the relative strength of adsorption on different adsorbents is highly dependent on the relative polarizability and electrostatic field strengths of adsorbent surface. These properties for some of common molecules are listed in the table (2.1). Often, considering these values help to predict accurate relative strengths of the amount adsorbed of given molecules on an

adsorbent or of the best adsorbent type (polar or nonpolar) for a particular separation.

Table 2.1 Electrostatic Properties of Some Common Molecules [2]

Molecule	Polarizability, $\alpha \times 10^{40}$, $(C^2.m^2/J^a)$	Dipole moment, $\mu \times 10^{30}$, $(C.m^b)$	Quadrupole moment, $Q \times 10^{40}$, $(C.m^{2c})$
Ar	1.83	0.00	0.00
H_2	0.90	0.00	2.09
N_2	0.78	0.00	-4.91
O_2	1.77	0.00	-1.33
CO	2.19	0.37	-6.92
CO_2	3.02	0.00	-13.71
CS_2	9.41	0.00	12.73
N_2O	3.32	0.54	-12.02
NH_3	2.67	5.10	-7.39
C_2H_6	4.97	0.00	-3.32
C_6H_6	11.49	0.00	-30.7
HCl	2.94	3.57	13.28

The selectivity, α, of a binary gaseous mixture including gas A and gas B in the Henry's region is defined as the ratio of the Henry's law constants of both gases.

$$\alpha(A/B) = \frac{K_A}{K_B} \tag{2-12}$$

Where, K_A and K_B are Henry's constant of species A and B, respectively.

In zeolites, selectivity shown towards particular adsorbate molecules may be modified by methods which change energy of interaction terms. Basically, three methods are known for changing the adsorption selectivity:

1. By preloading or introducing small amounts of a polar adsorbate such as water; which means water will preferentially adsorb on the most energetic sites in the zeolite strongly enough that it may not let other less selective adsorbate molecules replace it.

2. By cation exchange; cation exchange not only can change the pore size, but also it can affect the local electric field as well as adsorbate polarization.

3. Decationization; by removing all the cations present in the zeolite framework, the local electric field and field gradients will change.

22

Consequently, any interaction with a molecule with a permanent electric moment will be reduced.

2.4 Heat of Adsorption

All the adsorption processes which involve physical adsorption are exothermic and release heat. For adsorption to happen, the Gibbs free energy changes must be negative. From the thermodynamic relation point of view:

$$\Delta G = \Delta H - T\Delta S \qquad\qquad (2\text{-}13)$$

From the equation (2-13) it can be seen that the change in enthalpy, *ΔH*, is negative since the change in entropy, *ΔS*, is negative because the adsorbate molecules are in a more ordered configuration than in the phase gas. There are three terms referring to the heat of adsorption, including:

1. The isothermal integral heat of adsorption. This is the total heat released when the adsorbate loading is increased from zero to some final value at isothermal conditions.

2. The differential heat of adsorption, $\overline{\Delta H_1}$. This is the change in the integral heat of adsorption with a change in adsorbate loading. It may be defined by the following equation:

$$\overline{\Delta H_1} = (\bar{H}_1 - \tilde{H}_g) \qquad\qquad (2\text{-}14)$$

In which, $\tilde{H}_g$ and $\bar{H}_1$ are molar enthalpy and partial molar enthalpy of the gaseous adsorbate, respectively. The differential heat of adsorption depends upon pressure, temperature, and adsorbate coverage or loading.

3. The isosteric heat of adsorption, q_{iso} is derived from adsorption isosteres. It is achieved from a plot of the slopes of the adsorption isosteres (lines of constant adsorbate loading) on the graphs of the ln*P* vs. *1/T* through the Clausius-Clapeyron relationship:

$$\frac{dlnp}{d(1/T)} = -\frac{q_{iso}}{R} \qquad\qquad (2\text{-}15)$$

Where, R is the gas constant, P refers to the adsorbate absolute pressure, and T is the absolute temperature. The isosteric heat of adsorption is related to the differential heat of adsorption:

$$-q_{iso} = \overline{\Delta H}_1 \qquad\qquad (2\text{-}16)$$

It can be implied that the isosteric and differential heats are identical. It is possible to calculate the integral heat of adsorption from isosteric heats.

In most of the zeolites, at low loadings, a decrease in the heat of adsorption towards increasing in the adsorbate loadings has been observed. This is evidence to the fact that the adsorbent surface is energetically heterogeneous which means some of the adsorption sites interact more strongly with adsorbate molecules. These sites are filled first so that adsorption of additional molecules involves progressively lower heats of adsorption. All practical adsorbents have surfaces that are heterogeneous both energetically and geometrically (not all pores have uniform and constant dimensions). The degree of heterogeneity differs substantially from one adsorbent type to another. These heterogeneities are in charge of many nonlinearities, both in single component isotherms and in multicomponent adsorption selectivites.

2.5 Mechanisms of Gas Separation

Gaseous mixtures can get split employing adsorptive separation based on one or a combination of the three distinct mechanisms [5, 6]:

1. Steric Separation

2. Equilibrium Separation

3. Kinetic Separation

2.5.1 Steric Separation

Molecular sieving property of the zeolites accounts for steric separation. In other words, in the steric separation, the porous adsorbent has pores with special dimension such that it allows only small and properly-shaped molecules to enter, while prevents other molecules which do not fit the pores (different in size or geometry). Steric separation is restricted to the zeolites owing to their unique characteristics of having uniform micropores in their crystalline structures. One of the methods to control the aperture dimension is to exchange the cations in the zeolitic framework. For instance, zeolites 3A, 4A, and 5A which are three different cation-exchanged forms of zeolite A have distinct pore sizes which allow them to adsorb molecules with effective diameters smaller than 3 Å, 4 Å, and 5 Å respectively. Drying with 3A zeolite and the separation of normal paraffins from iso-paraffins and cyclic hydrocarbons using 5A are the two largest applications of steric separation [5, 6].

2.5.2 Equilibrium Separation

Equilibrium mechanism which is used in most of the gas adsorption processes is thermodynamically driven. It is operating through the differences in the interaction energies between the competitive adsorbates and the adsorbent, which means the stronger adsorbing species preferentially adsorbs on the adsorbate surface [5, 6]. Oxygen generation from air employing zeolite Li-LSX is an example of equilibrium separation. At equilibrium, nitrogen has higher interaction affinity on zeolite Li-LSX than that of oxygen. Therefore, when air is passing through the adsorbent, nitrogen adsorbs and a pure stream of oxygen can be obtained [3, 5].

2.5.3 Kinetic Separation

Kinetic mechanism is based on the differences in the diffusion rates of various adsorbate species to get into the adsorbent pores [6, 7]. Therefore, by controlling the exposure time of the gaseous species to the adsorbent, the faster diffusing

molecule would be selectively adsorbed on the adsorbent surface. Unlike equilibrium separations in which equilibrium interaction energies of the adsorbate account for the separation, in kinetic separation difference in the rate of adsorption can be used to design a separation system. The only class of molecular sieves which operate through the kinetic separation is carbon molecular sieves (CMS) because they have a distribution of pore sizes as shown in Figure (2.2). This means that having such distribution of pores not only allows diffusion of different gases at different rate, but also avoids exclusion of any gases in the mixture. Nitrogen production from air is a commercial example of kinetic separation using CMS [5]. Oxygen can diffuse much faster than nitrogen which is believed to be as a result of smaller kinetic diameter of oxygen compared to nitrogen. Therefore, although CMS has a smaller capacity compared to most of the other zeolites, it is more efficient to use CMS for nitrogen generation from air.
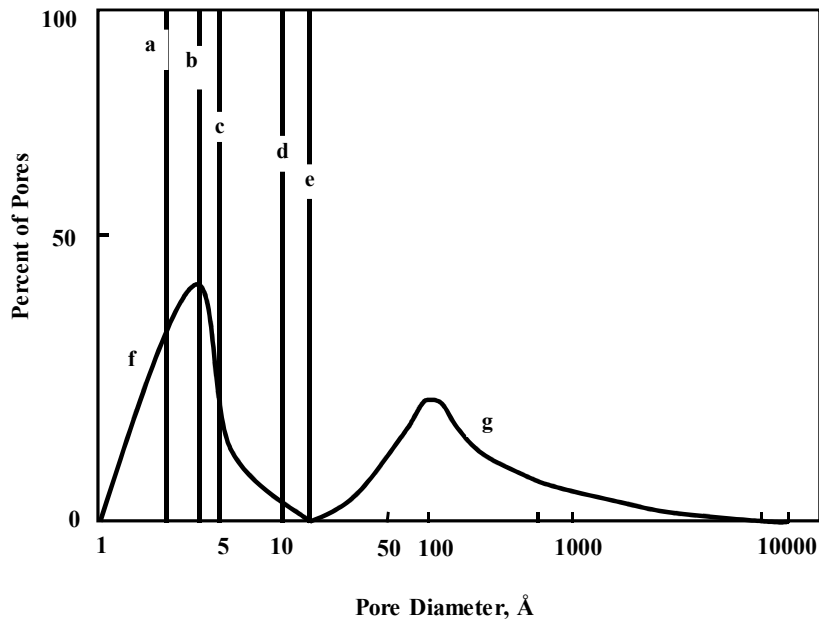
Figure 2.2 Micropore size distributions of (a) zeolite 3A, (b) 4A, (c) 5A, (d) 10X, (e) 13X, (f) CMS, and (g) activated carbon

26

2.6 Equilibrium Adsorption of Single Gases

For a given gas-solid pair, the amount of gas adsorbed on the adsorbent at equilibrium is a function of temperature, T, and pressure, P, which can be defined by:

$$\upsilon = f(P,T) \tag{2-17}$$

Where, υ may be stated in STP cc/g. As can be seen from this equation, at a fixed temperature, υ is only a function of the pressure. This is a prerequisite for the design of the adsorptive processes and called adsorption isotherm.

2.6.1 Approaches for Isotherm Models

Brunauer classified the commonly observed forms of isotherms into the five types depicted in Figure (2.3).
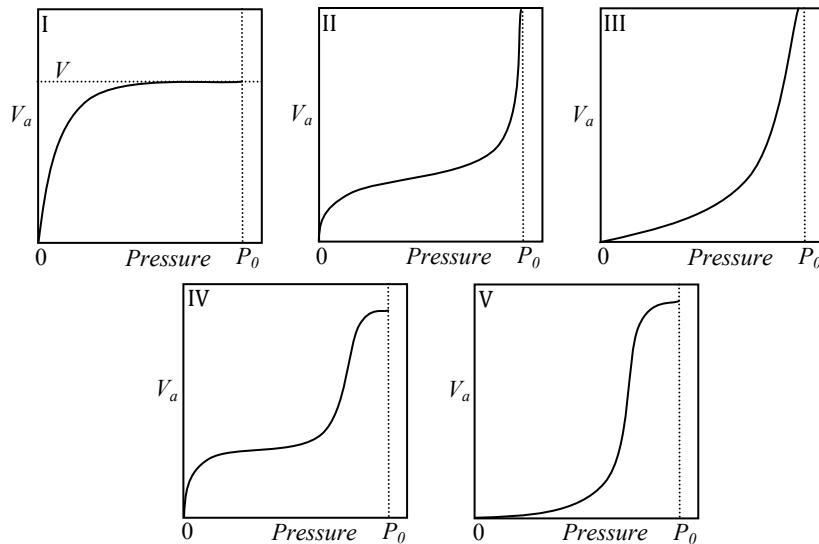
Figure 2.3 The Brunauer classification of the adsorption isotherms [3]

Isotherm type (I) illustrates Langmuir isotherm (monolayer coverage) that is characteristic of chemisorption in which the saturation limit corresponds to occupation of only all surface sites, or to physisorption in a microporous material

27

where the saturation limit corresponds to complete filling of the micropores. Type (II) isotherm demonstrates BET mechanism for multi-layer adsorption. Types (I) and (II) are the most frequently encountered in separation processes. Type (III) corresponds to cases where adsorbate-adsorbent interaction is weaker than that of adsorbate-adsorbate; adsorption of H_2O on the charcoal surface can be mentioned as an example of this kind of behaviour. While, this adsorption is not favourable at low pressure due to the nonpolar (hydrophobic) nature of the charcoal surface, at sufficiently high pressures, the adsorption is due to capillary condensation in the mesopores of charcoal. Types (IV) and (V) are same as types (II) and (III) except that they have finite adsorbed capacity limits as P approaches the saturation pressure (P_0) due to the finite pore volume of the porous solids. The following examples typify the five mentioned classes of isotherms:

Type (I): Adsorption of oxygen on charcoal at 90 K

Type (II): Adsorption of nitrogen on ironic catalysts at 78 K

Type (III): Adsorption of bromine on silica gel at 352 K

Type (IV): Adsorption of benzene on ferric oxide gel at 323 K

Type (V): Adsorption of water on charcoal at 373 K

The great majority of the isotherms models are established based on three different approaches:

1. *The Langmuir Approach:* Langmuir approach which is proposed by Langmuir (1918) [5] is based on kinetic adsorption and assumes that adsorption system is in dynamic equilibrium, and the evaporation rate (desorption) is equal to that of condensation (adsorption). Langmuir approach is the most practical method in data correlation in separation processes.

2. *The Gibbs Approach:* Gibbs (1928) [1], supposed that adsorbent is thermodynamically inert at equilibrium. Gibbs adsorption isotherm equation is applied in this approach which assumes a two-dimensional equation of state of the adsorbed film, relating π-A-T:

$$-Ad\pi + nd\mu = 0 \qquad\qquad (2\text{-}18)$$

In which, π is the spreading pressure, A is surface area, n and μ are the number of moles and the chemical potential, respectively. An integration of the Gibbs equation results in the desired isotherm. There are as many isotherms as the number of assumed equations of state, ranging from the ideal gas law to virial equations, which are truncated at a certain point [8].

3. *The Potential theory:* According to this theory which was first developed by Polanyi in 1914 [5], in the adsorption system, gas molecules concentrate gradually on the solid surface owing to the potential field (which is similar to atmosphere of the planet). For a given gas-solid system, there is an empirical relationship called "characteristic curve":

$$w = f(\varepsilon) \qquad\qquad (2\text{-}19)$$

Where, ε stands for potential field and w refers to the volume above the surface. It is believed that characteristic curve relationship is independent of temperature so that it is essentially an isotherm equation. The adsorption potential is defined as the work of the isothermally compression of the gas from its pressure (P) to the saturation pressure (P_0) for the liquefaction. Assuming the adsorbed phase to be liquid, the volume (w) will be the amount adsorbed and then adsorption isotherm is achieved.

As mentioned before, these three approaches are being applied to derive different isotherm models. For instance, Langmuir isotherm, Langmuir isotherm with Lateral interactions, Freundlich isotherm, BET isotherm are all based on Langmuir approach. Harkin-Jura and Polanyi-Dubinin isotherms are developed by making use of the Gibbs equation.

2.6.2 Langmuir Isotherm

This isotherm is the simplest and the most practical one and can be employed for both physical and chemical adsorption processes. Implicit assumptions made in arriving at the Langmuir isotherm are:

1. Adsorption is mono-molecular layer.

2. Adsorption is localized, that is adsorbate molecules remain at the site of adsorption until adsorbed.

3. The energy of adsorption is independent of the surface coverage and stays constant over all sites.

This isotherm is formulated based on a dynamic equilibrium between the adsorbed phase and gaseous phase. It was supposed that the rate at which adsorbate gas molecules strike a surface of the adsorbent (adsorption) is proportional to the product of the partial pressure p of the gas and the fraction $(1-\theta)$ of the surface remaining uncovered by adsorbate and is available as adsorption sites. In addition, the rate of desorption from the surface is supposed to be directly proportional to the fractional surface coverage θ. Since the rate of the adsorption and desorption are equal at equilibrium, thus:

$$k_a \, p \, (1 - \theta) = \; k_d \theta \qquad\qquad (2\text{-}20)$$

Where, k_a and k_d are rate of adsorption and desorption, respectively. The more useful from of the equation is:

$$\theta = \; q/q_m = \; bp/(1 + bp) \qquad\qquad (2\text{-}21)$$

Where, b is k_a/k_d and q is the quantity of gas adsorbed and q_m is the maximum amount adsorbed which is a single monolayer.

It is assumed that a single molecule occupies a single surface site and there is no lateral interaction between adjacent adsorbed molecules. Application of the kinetic theory of gases reveals that the constant b can be identified as:

$$\frac{1}{b} = \frac{v}{\sigma}(2\pi mkT)^{1/2}exp\left(-\frac{Q}{R_gT}\right) \qquad (2\text{-}22)$$

Where, v is the pre-exponential factor of the desorption coefficient, σ is the condensation (adsorption) coefficient which is defined as the fraction of adsorbed molecules with activation energy greater than heat of adsorption (E_a). m and k are the mass of the adsorbate molecule and the Boltzmann constant, respectively. Q refers to the heat of adsorption which is the difference between the activation energies E_d and E_a necessary for desorption and adsorption, respectively.

2.6.3 Henry's Law

At low pressures when pressure approaches zero, Langmuir equation (2-21) reduces to a linear form called Henry's Law:

$$q = q_mbp = Kp \qquad (2\text{-}23)$$

Where, the proportionality constant, K is the Henry's law constant which is the adsorption equilibrium constant that decreases with increasing temperature. The dependence of Henry's law constant to the temperature can be described by the Van't Hoff relationship:

$$K = A\,exp(-\Delta H/RT) \qquad (2\text{-}24)$$

In which, A is the pre-exponential factor, ΔH is heat of adsorption, R and T are the gas constant and the absolute temperature, respectively.

2.6.4 Freundlich Isotherm

For many systems there is ample evidence to show that the heat of adsorption drops in magnitude as the amount of adsorption increases. Zeldowitch (1935) made an assumption that if the decrease in heat of adsorption is logarithmic, it indicates that adsorption sites are non-uniform and they are distributed exponentially with respect to adsorption energy which is different between groups of adsorption site. In other words, unlike the Langmuir isotherm, heat of

adsorption varies with coverage and doesn't show an adsorption limit when coverage is sufficient to fill a monolayer ($\theta = 1$). The following classical empirical equation defines Freundlich isotherm:

$$\theta = kp^{1/n}, \quad n > 1 \tag{2-25}$$

2.6.5 Brunauer-Emmett-Teller (BET) Isotherm

The Brunauer-Emmett-Teller (BET) equation which is originally proposed by Brunauer, Emmett, and Teller (1938) [1, 3] is commonly applied to evaluate specific surface area. This model is based on the assumption of multilayer adsorption on a flat surface. The BET model is based on that of Langmuir for monolayer adsorption except that the BET model considers the formation additional layers after forming the monolayer in situations where the temperature is below the critical temperature of the gaseous adsorbate. According to the BET, molecules adsorbed in one layer are considered as adsorption sites in the next layer, consequently a large number of the layers can be adsorbed on the surface and leads to the notion of a statistical monolayer. Like Langmuir assumptions, in the BET it is assumed that there is only one type of adsorption site and there are no lateral interactions between adsorbed layers. The other assumption that was made is that the characteristics of the second and following layers are same as that of the bulk fluid phase.

In the BET model, *0* to *i* (*i* approaches infinity) non-mobile adsorbate molecules can be accommodated by each site on the adsorbent surface. On the first layer, the rate of condensation on the vacant sites is equal to the rate of evaporation from the sites that are covered by only one adsorbate molecule. Following this approach, *i* equations are generated when equilibrium is established for all layers. The important assumption made in this model is that the heat of adsorption of the first layer E_1 is considered to be different from that of further layers. And the heat of adsorption of all the layers except first layer is assumed to be constant and equal to the heat of liquefaction, E_L. Furthermore, the ratio of the adsorption and desorption constants, α/β, is also assumed constant for

the layers beyond the first layer. Therefore, the BET equation is achieved by summing over all the layers:

$$\frac{P}{v(P_0 - P)} = \frac{1}{v_m c} + \frac{c-1}{v_m c}\left(\frac{P}{P_0}\right) \qquad (2\text{-}26)$$

Where the amount of c is given by:

$$c = \frac{\alpha_1 \beta_2}{\alpha_2 \beta_1} exp\left(\frac{Q_1 - Q_L}{RT}\right) \cong exp\left(\frac{Q_1 - Q_L}{RT}\right) \qquad (2\text{-}27)$$

In the equation (2-27), subscripts indicate the number of layers starting from the surface, and L denotes for liquefaction. The values of c and v_m are experimentally determined. The constant c is usually large and always greater that one. The BET equation is still a very powerful tool to measure the surface area of the porous solids. Using the data in the range of $0.05 < P/P_0 < 0.3$, by plotting the left side of the equation (2-26) against the relative pressure, the values of c and v_m are obtained from the intercept and slope of the plot. Then, by knowing the molecular area of the adsorbed molecule (e.g. 16.2 $Å^2$/molecule of nitrogen at 77K), the amount of the surface area can be found directly from v_m.

The BET equation is rarely used to correlate adsorption data. This is not only because of its mathematically complexity, but also it is not applicable to adsorption under supercritical conditions. Under these conditions, the BET model reverts to Langmuir model.

2.7 Equilibrium Adsorption of Gas Mixtures

Finding right models or correlations for gaseous mixtures is of high importance due to their crucial role in the design of adsorptive gas separation processes. These models should be able to predict the adsorption properties of a multicomponent gaseous mixture equilibrium employing single-component adsorption data in a given ranges of operating temperature and total pressure. The methods used to obtain single-component experimental isotherms may also be employed to collect data for multicomponent isotherms with an additional assumption. Correlations based on the Langmuir, Polanyi, and Gibbs approaches

for single gases adsorption has been applied for multicomponent gaseous mixtures and different isotherm models using these approaches have emerged [6, 9].

2.7.1 Extended Langmuir Isotherm

Langmuir isotherm can be simply extended to a relation for a multicomponent gaseous mixture only by adding one more assumption to those mentioned for single-gas component Langmuir isotherm, that for every gaseous component there is an equilibrium between the amount adsorbed at the adsorbent surface and its partial pressure in the gas phase. Fractional coverage θ_i and partial pressure p_i are attributed to each of the components in the adsorbed and gaseous phase, respectively. The total surface coverage is sum of coverage of the individual component which the resulting Langmuir isotherm for component i can be defined as:

$$\theta_i = \frac{q_i}{q_{mi}} = \frac{b_i p_i}{1 + \sum_1^n b_i p_i} \qquad (2\text{-}28)$$

In which, q_{mi} is the maximum amount of component i (monolayer) from a gaseous mixture adsorbed on the adsorbent. And the total surface coverage is:

$$\theta_{Total} = \sum_{i=1}^{n} \theta_i \qquad (2\text{-}29)$$

Extended Langmuir isotherm is extensively used for modeling of pressure swing adsorption processes mostly due to its simplicity. In addition, PSA processes work under conditions where the loading is very low ($q/q_s<0.5$) which under these conditions, Langmuir model is relatively accurate.

Recognizing the deficiency of the extended Langmuir equation, despite its strong basis of thermodynamics and kinetics theories, other methods such as the ideal adsorbed solution theory of Myers and Prausnitz [3, 5], the real adsorption theory, the vacancy solution theory and the potential theory have been proposed.

2.7.2 Ideal Adsorbed Solution Theory (IAST)

Ideal Adsorbed Solution Theory (IAST) is based on the assumption that the adsorbed phase is thermodynamically ideal and in equilibrium where the chemical potentials of both adsorbed phase and gas phase must be equal [1]. The partial pressure exerted by component *i* in the gaseous mixture can be defined as:

$$p_i = p_i^o(\pi)x_i \tag{2-30}$$

Where, $p_i^o(\pi)$ is the saturated vapour pressure of component *i* in its pure state at the same spreading pressure of the adsorbed phase (π) and same temperature, and x_i stands for the mole fraction of species *i* in the adsorbed phase. Equation (2-30) is equivalent to Raoult's law for ideal liquid-vapour systems. For a case where the mole fraction of species *i* in the gas phase is y_i and total pressure of the system is *P*, in equilibrium the relation between gas phase and adsorbed phase becomes:

$$y_i P = p_i^o(\pi)x_i \tag{2-31}$$

Therefore, in case of equal spreading pressures in a mixture, the condition $\pi_i = \pi_j = \pi_{mix}$ must be obeyed. Now to relate spreading pressure to moles adsorbed we need to use equation (2-18) from Gibbs approach and by substituting the classic thermodynamic relation for $\mu(p)$ for the gas phase at pressure *p*,

$$d\mu = R_g T dlnp \tag{2-32}$$

In which, *p* is the partial pressure of the adsorbate, and then by substituting equation (2-32) in (2-18), we will have:

$$Ad\pi = nR_g T dlnp \tag{2-33}$$

This equation is the differential form of the Gibbs equation isotherm which in its integral form becomes:

$$\pi = R_g T \int\limits_{0}^{p_s} (n/A)\, dlnp \qquad\qquad (2\text{-}34)$$

Using equation (2-34) for a mixture composed of components *i* and *j*:

$$\pi A / R_g T = \int\limits_{0}^{p_i^o} n_i^o(p)\, dlnp = \int\limits_{0}^{p_i^o} n_j^o(p)\, dlnp \qquad\qquad (2\text{-}35)$$

Where, $n^o{}_i(p)$ and $n^o{}_j(p)$ are the isotherms for the pure component *i* and pure component *j*, respectively. Worth to mention that in all above equations, the following relation between mole fractions of components in both adsorbed and gas phase is valid:

$$\sum x_i = \sum y_i = 1 \qquad\qquad (2\text{-}36)$$

Assuming the total pressure, *P*, and mole fraction of the component *i* in the gas phase, y_i, are known, then the calculation procedure for the binary mixture would be to find p_1^o, p_2^o, and x_1 from the three equations (2-30), (2-31), and (2-36). Once values for p_1^o, p_2^o, and x_1 have been found, n_1 and n_2 may be calculated. The similar procedure would be followed for multicomponent mixtures [1].

2.8 Adsorption Gas Processes

Adsorption equipment and operating cycles usually can be designed reliably on the basis of the measured adsorption isotherm data and reasonable number of relatively small-scale experiments to predict the mass transfer characteristics of the feed stream to be treated in the chosen adsorbent bed. Chemical adsorption can be divided into two categories [3, 5]:

- *Bulk separation*: in which about 10 *wt.* % or more of the gas stream must be adsorbed.

- *Purifications*: in which usually significantly less than 10 *wt.* % of feed stream must be adsorbed.

It is worthwhile to know the difference between these categories since they generally need different adsorption processes. Adsorption processes are often classified based on the method of adsorbent bed regeneration. Pressure swing adsorption (PSA) and temperature swing adsorption (TSA) are the most frequently used processes. In addition, some other adsorption processes such as purge swing cycles and non-regenerative approaches are also applied [3, 5].

2.8.1 Gas Chromatography

Gas chromatography (GC) has been a common laboratory analytical technique for over a quarter of a century. It has been an appealing tool for large scale commercial processes due to sharp separation which often can be obtained from GC. The basic mechanism of separation is same as that of analytical chromatography but as it is scaled up to industrial scales, some problems appear due to using larger amounts of sample and larger columns. The successful GC process scale-up means that two probable crucial problems which are flow mal-distribution (that results in the reduction in the number of possible theoretical stages) and capacity limiting thermal gradient of the adsorbent have been solved [3, 5].

In the GC column, the solubility of each component in the gas phase depends on its vapor pressure, which is in turn a function of the column temperature and the affinity between the compound and the stationary phase. Differences in vapor pressure result in partitioning of the molecules of each component between the mobile and stationary phase. When a molecule enters the gas phase it is swept towards the detector by the carrier gas flow. Consequently, compounds with different physical and chemical properties will arrive at the detector at different times. The stationary phase can be a solid or liquid coating an inert solid support; this gives rise to two forms of gas chromatography; gas-solid (GSC) and gas-liquid (GLC) chromatography.

2.8.2 Pressure Swing Adsorption

In pressure swing adsorption (PSA) processes [2], the regeneration of the adsorbent during desorption cycle is achieved by dropping the total pressure of the system and purging the bed at lower pressure. PSA processes are principally used for bulk separations where there are high concentrations of contaminants. Systems with weakly adsorbed species are especially suited for PSA. The PSA cycles are characterized by high residual loadings and low operating loadings. Figure (2.4) demonstrates the operating loading (X_1-X_2) that arises from the partial pressure at feed conditions and the lower total pressure of desorption step (P_2), the greater the operating loading.
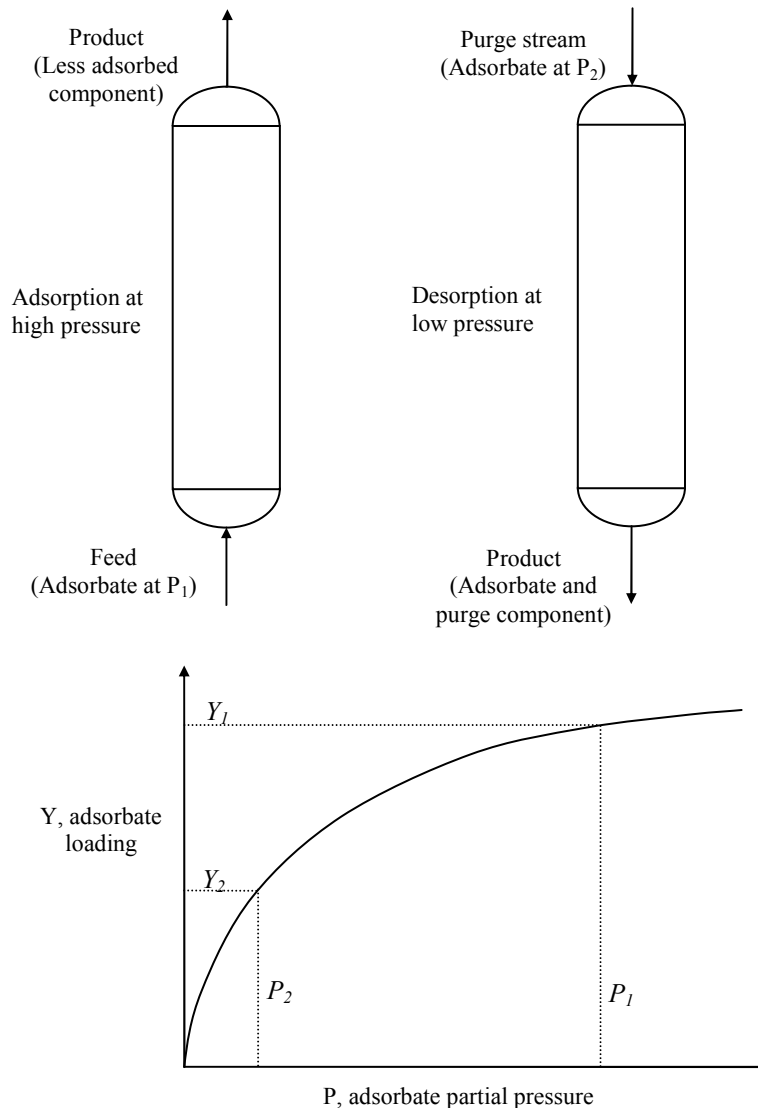
Figure 2.4 Pressure swing adsorption cycle

Every PSA unit mainly consists of four steps, loading, depressurizing, regenerating, and repressurizing. The time required for these four steps is usually a few minutes. Different applications may need different additional steps. Systems with weakly adsorbed species are especially suited for PSA. Drying, upgrading of H_2 and fuel gases, and air separation are some of the applications of PSA units. Packed bed of adsorbent responds rapidly to changes in pressure and purge stream usually removes the desorbed components from the bed, and then the bed is returned to adsorption conditions by repressurization. During regeneration in a PSA, two processes occur: depressurizing and purging. In depressurizing, the reduction in the operating pressure must be low enough to allow desorption of the adsorbates to happen. And enough purge gas must flow through the bed to remove the desorbed species from the adsorbent bed. Equilibrium defines the maximum possible gas capacity on the bed to achieve. These cycles operate at almost constant temperature and it needs no heating or cooling steps and the exothermic heat of adsorption is held in the adsorbent to provide the required endothermic heat of desorption.

In general, pressure swing adsorption cycles are categorized in three classes based on the operating pressure range as PSA, VSA (vacuum swing adsorption), PSPP (pressure swing parametric pumping) or RPSA (rapid pressure swing adsorption). While, PSA swings between a high and a low super-atmospheric pressure, VSA swings from a super-atmospheric pressure to a sub-atmospheric pressure. Otherwise, the principles involved in these methods are the same.

2.8.3 Temperature Swing Adsorption

In temperature swing adsorption (TSA) processes [2] desorption occurs at a temperature much higher than that of adsorption. The principle application of TSA is purification which means the systems in which the concentration of contaminants is very low. The characteristic of TSA cycles is that the residual loadings are low and operating loadings are high. The isotherms for two

temperatures of a TSA cycle are illustrated in Figure (2.5). The difference between the loadings X_1 and X_2 stands for the available operating capacity. For reasonably sized bed, these high adsorption capacities for low concentrations means that cycle times are hours to days. Due to slow response of the packed adsorbent bed to the changes in gas temperature, this long cycle time is favourable. Purging removes the thermally adsorbed components from the bed and then by cooling the bed, it is returned to the adsorption condition. Unlike PSA unit which were suitable for weakly adsorbed species, TSA units are the best option for systems in which adsorbates are strongly stuck on the adsorbent such as drying, sweetening, CO_2 removal, and pollution control.

In a TSA cycle principally two processes take place during regeneration including, heating and purging. Throughout heating, thermal energy must be adequate to be able to raise the temperatures of adsorbate, adsorbent, and adsorber high enough to desorb the adsorbate and make up for heat losses. When transfer of the energy to the system is limiting, the regeneration is heating limited. After heating, purge gas flows to remove desorbed species from the adsorber. Equilibrium determines the maximum capacity of the purge gas to remove the desorbed material. Regeneration is stripping limited when transferring adsorbate away is limiting. Heating occurs by either direct contact using external heat exchange to the purge gas or indirect contact applying coils inside the adsorber. After the heating step, cooling is done to reach the temperature of the bed to the adsorption temperature.

Although thermal swing regeneration can be done at same pressure as adsorption, lowering the pressure commonly used to achieve better desorption. Such cycles are actually a hybrid of PSA and TSA referred to as pressure/ thermal swing adsorption (PTSA). The heating gas is normally used for the cooling step. By the way, rather than cooling the bed, adsorption can sometimes be started on hot bed.
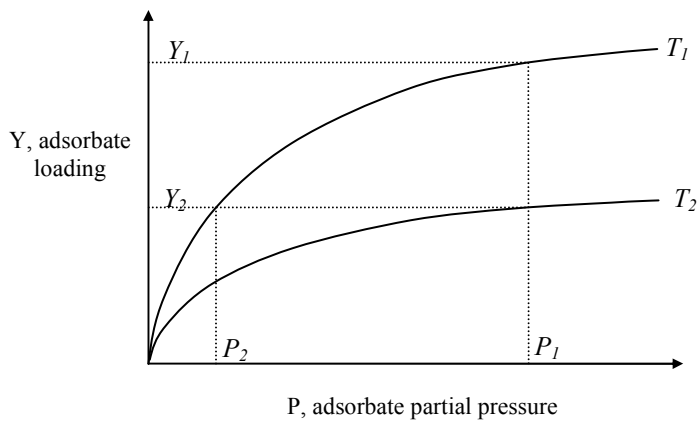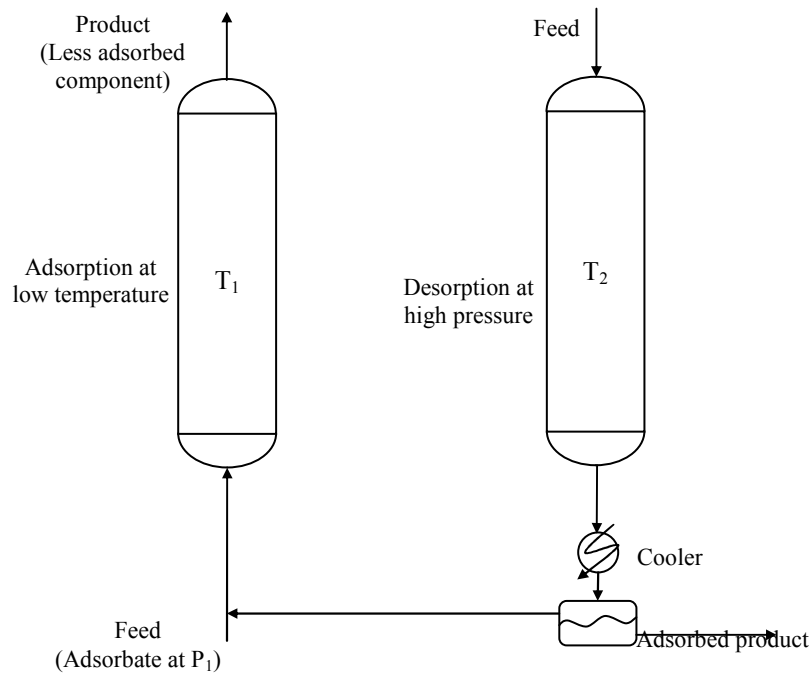
Figure 2.5 Temperature swing cycle

References:

[1] W. J., T., and Barry, C., 1998, "Adsorption Technology and Design", Elsevier Science & Technology Books.

[2] Kirk, R.E., 2003, "Adsorption, Gas Separation. Kirk-Othmer Encyclopedia of Chemical Technology", John Wiley & Sons, Inc.

[3] Yang, R.T., 2003, "Adsorbents : fundamentals and applications", Wiley-Interscience.

[4] Breck, D.W., 1974, "Zeolite molecular sieves: structure, chemistry, and use", Wiley, New York.

[5] Ralph T. Yang, 1987, "gas separation by adsroption processes", Butterworth, Boston.

[6] Duong, D.D., 1998, "Adsorption analysis : equilibria and kinetics", Imperial College Press.

[7] Chen, N., and Yang, R. T., 1996, "Ab Initio Molecular Orbital Study of Adsorption of Oxygen, Nitrogen, and Ethylene on Silver-Zeolite and Silver Halides", Industrial & Engineering Chemistry Research, 35(11) pp. 4020-4027.

[8] Gaskell, D.R., 2008, "Introduction to the thermodynamics of materials", Taylor & Francis.

[9] Ruthven, D.M., 1984, "Principles of Adsorption and Adsorption processes", John Wiley & Sons, Inc., Canada.

Chapter 3

Silver Chloride Filament Growing on ETS–10

3.1 Introduction

Nanosilver materials are being used for different purposes such as medical applications [13], catalysis [14-16], separation [17-22], and mercury removal [23, 24]. Due to their importance, extensive studies have been carried out to investigate various possible methods to synthesize silver nanoparticles in a variety of sizes and shapes such as disks [1-3], rods [4], prisms [5-9], wires [10-12]. Different proposed methods to fabricate metal nanoparticles include high vacuum approaches, sol-gel synthesis [13-15], a range of photochemical [6, 7], and thermal processes [8, 16-18], as well as plasma-polymerization [19]. A newly developed technique is based on exploiting zeolite surfaces to induce the formation of metal nanostructures or zeolite supported metallic nanodots [20-23]. According to Tsapatsis [24], molecular sieves are the best potential candidates to contribute to nanotechnology needs due to their unique properties on a nano and subnano dimensional scale materials. A major feature of zeolites which differentiates them from other matrices with non-regular structures is the presence

of well-ordered intracrystalline cavities. Metallic nanodots and clusters can be incorporated and stabilized in these zeolitic channels and their size is more dependent on the zeolite type rather than composition and SiO_2/Al_2O_3 molar ratio. In the case of zeolite mordenite, silver metals can be produced in both mono-sized aggregates and nano-ranged particles owing to zeolite mordenite's silica to alumina ratio [25, 26]. Traditional methods for generating silver nanoparticles are expensive and they usually require using harmful chemicals. These techniques are highly dependent on temperature and duration of reaction. In general, they are slow (more than 20 hours) but the time can be reduced by applying heat which would add to the energy cost. In contrast, zeolite supported metallic nanodots can be simply produced by the ion exchange of zeolites with a solution of metal ions (at 80° C with stirring for 1 hour) followed by the reduction of the products in a reducing environment. Under certain conditions, few sub-nanometer silver clusters can be formed inside the zeolitic cavities and under reductive environments larger agglomerates can often generate outside of them [25, 26]. The dimensions of the zeolitic channels for typical zeolites are in the range of 5–12 Å which determines the upper limit of the cluster sizes allowed to be stabilized inside the cavities without changing the zeolite crystalline framework. This means that silver metal nanoparticles of sizes bigger than limits can only be localized at the surface of the zeolite microcrystals [22, 23, 25-29]. Since silver metals are highly mobile on the zeolite surfaces, stabilizing the metal nanoparticles in the zeolite frameworks is challenging. Typically, a silver metal nanodot material is generated by ion exchange followed by reduction. As they are heated during the reduction step, silver metals present in the zeolite framework tend to migrate to the zeolite surface and come together to form micron-scale agglomerates and there is only a trace of nanodots on the surface. Since these clusters have lower surface to volume ratio than that of nanodot ensembles, they generally exhibit the behaviour of bulk metals and not the unique characteristics of the nanoparticles [22, 23, 25-29]. Unlike zeolite molecular sieves where silver nanoparticles grow mostly inside their frameworks, metallic nanoparticles form on the surface of ETS molecular sieves supports. It is believed that after reduction, silver ions travel to

the ETS zeolite surface and stay as nanoparticles instead of agglomerating to large sheets or ensembles [23]. The exact mechanism of this phenomenon is not clear, but the size and even distribution of silver nanodots are probably due to the ability of ETS molecular sieve surface to pull nonpolar species such as a pure metal particle. Consequently, pure metals tend to stick to the surface of the ETS molecular sieve surface [23].

Silver ions convert to metallic silver nanodots supported on the ETS zeolite, by an activation step which consists of drying at different elevated temperatures from 75° C to about 400° C. It appears that silver nanoparticle's dimensions highly depend on activation step and the nature of the reducing or oxidizing environment during activation. Reducing conditions such as hydrogen results in the formation of large nanoparticles while oxidizing conditions such as oxygen or air, produces smaller nanodots [23, 30]. One of the most important applications of Ag–ETS–10 is in air separation and especially in the adsorption of noble gases such as Ar, Xe, and Kr. Due to similar physical properties of O_2 and Ar, generation of high purity of O_2 is a challenging process. When Ag–ETS–10 is used as an adsorbent, Ar atoms can attach stronger to the silver nanodots formed on the ETS–10 surface allowing some degree of selectivity towards Ar [31].

In this chapter, different experiments and methods were conducted to gain insight on the role of silver nanoparticles in air separation and especially in Ar and O_2 separation. By using chloride solutions as a silver scavenger on Ag-ETS-10, different levels of active silver concentration were obtained. This was confirmed by means of results from XRD and EDX techniques. The resulting effects on air and Ar/O_2 separation were studied by inverse chromatography.

3.2 Experimental Methods

ETS–10 Synthesis. ETS–10 was synthesized hydrothermally according to the procedure reported by Kuznicki [32]. In a typical synthesis, a mixture of 50 g of sodium silicate (28.8% SiO_2, 9.14% Na_2O, Fisher), 3.2 g of sodium hydroxide (97+% NaOH, Fisher), 3.8 g of KF anhydrous, Fisher, 4 g of HCl (1M), and

16.3 g of $TiCl_3$ solution (Fisher) was thoroughly stirred in a blender for 1 h, and then reacted in a 125 ml sealed autoclave (PARR Instruments) at 488K for 64 h. The resultant material was washed and vacuum filtered with de-ionized water, and dried in an oven at 373 K.

Silver Exchange. In order to prepare silver exchanged ETS–10, as synthesized Na–ETS–10 powder was exposed to an excess of aqueous solution of $AgNO_3$ (Fisher) at 353 K stirring for 1 hour. The exchanged materials were thoroughly washed and vacuum filtered with de-ionized water after each exchange and finally dried in the oven at 353 K.

Silver Ion Exclusion. To exclude silver ions and form silver chloride filaments, after activating Ag–ETS–10 at 473 K for 2 hours in the presence of air, it was exposed to a very concentrated aqueous solution of calcium chloride.

X–ray Powder Diffraction. Phase identification of the as-synthesized materials was conducted through XRD using a Rigaku Geigerflex 2173 with a vertical goniometer equipped with a graphite monochromator for filtration of K-β wavelengths.

Scanning Electron Microscopy. Scanning electron microscopic analysis (SEM) of the sodium- and silver-exchanged ETS-10 samples were carried out using a LEO 1430 VP variable-pressure scanning electron microscope.

Energy Dispersive X–ray. Energy Dispersive X–ray (EDX) data were collected using a JEOL JZA-8900R WD/ED Combined Microanalyzer. Signals were obtained from secondary electrons at an accelerating voltage of 15 kV.

Inverse Gas Chromatography Measurement. Inverse gas chromatography experiments (IGC) were performed using a Varian CP 3800 gas chromatograph (GC) equipped with a thermal conductivity detector (TCD). Typically, 3–4 g of adsorbent was packed into the copper columns with 10 inch length and one quarter inch OD. Installing the columns in the IGC, they were activated heating at 473 K for 16 h under 30 ml/min helium as a carrier gas flow. Test gases (Air, Ar, O_2 and 50–50% mixtures of Ar–O_2) were introduced into the column by a 1 mL

pulse injection at 303K. Such diluted system conditions allow estimating Henry selectivities providing there are no diffusion limitations and an isothermal plug flow model can be assumed [33]:

$$\alpha_{i/j} = \frac{t_i - t_0}{t_j - t_0} \qquad (3\text{-}1)$$

Where, t_0 stands for the residence time of the inert carrier gas which has no affinity to the packed bed column. t_i and t_j refer to the retention times of the eluting species.

3.3 Results and Discussion

The formation of AgCl filaments on ETS–10 framework. Silver–exchanged ETS–10 is activated by heating at 473 K for 2 hours in air which converts silver ions to metallic silver. They migrate to the ETS–10 surface resulting in silver nanodot formation on the surface.

When the Ag–ETS–10 is heated with a very concentrated aqueous $CaCl_2$ solution at 353 K, silver and chloride ions produce silver chloride that precipitates on the ETS–10 surface. Therefore, the silver ions removed by the formation of silver chloride are replaced by calcium in $CaCl_2$:

$$Ag_m - ETS - 10 + nCaCl_2 + nH_2O \rightarrow$$
$$Ag_{m-2n} - ETS - 10 + nCa^{2+} + 2nAgCl + nH_2O \qquad (3\text{-}2)$$
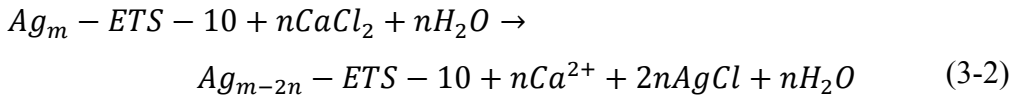
Figure (3.1) shows SEM image of as synthesized Na–ETS–10 with clean cubic crystalline structure.
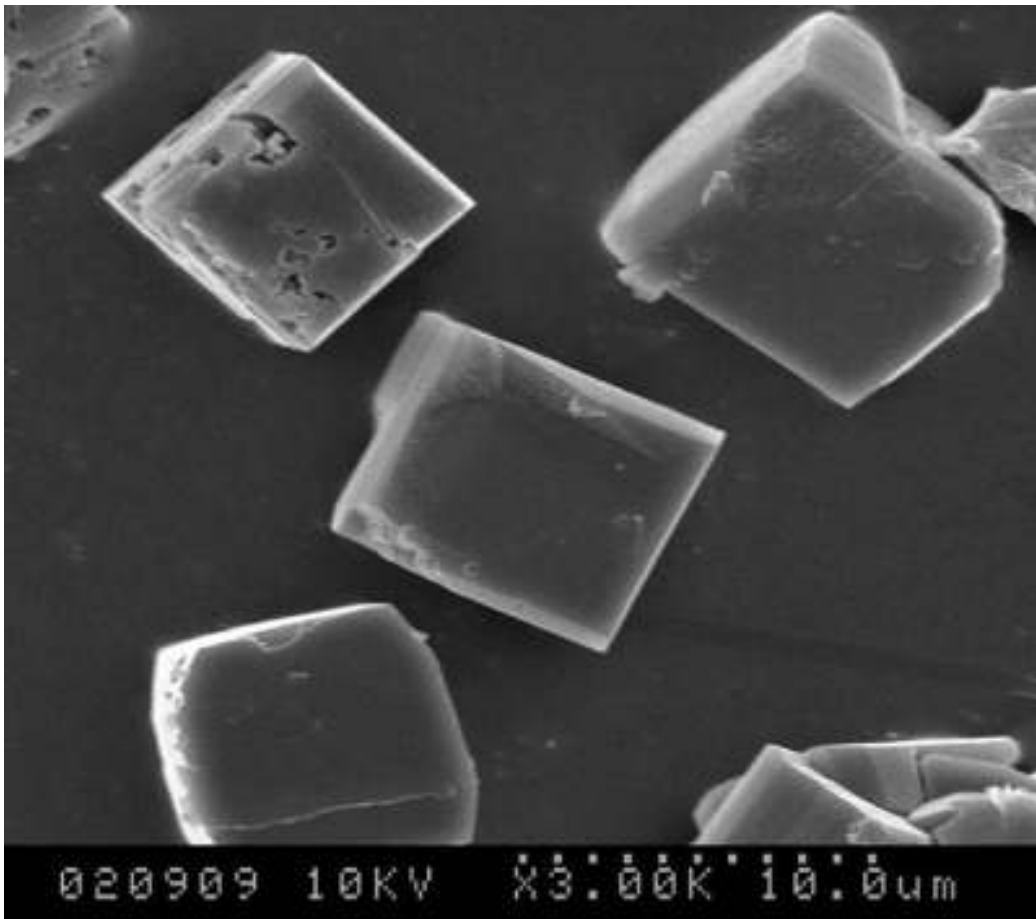
Figure 3.1 SEM image of as–synthesized Na–ETS–10 with crystalline cubic shape

SEM images of Ag–ETS–10 are shown in the Figure (3.2). The results show silver nanoparticles formed on the surface of the cubic crystals.
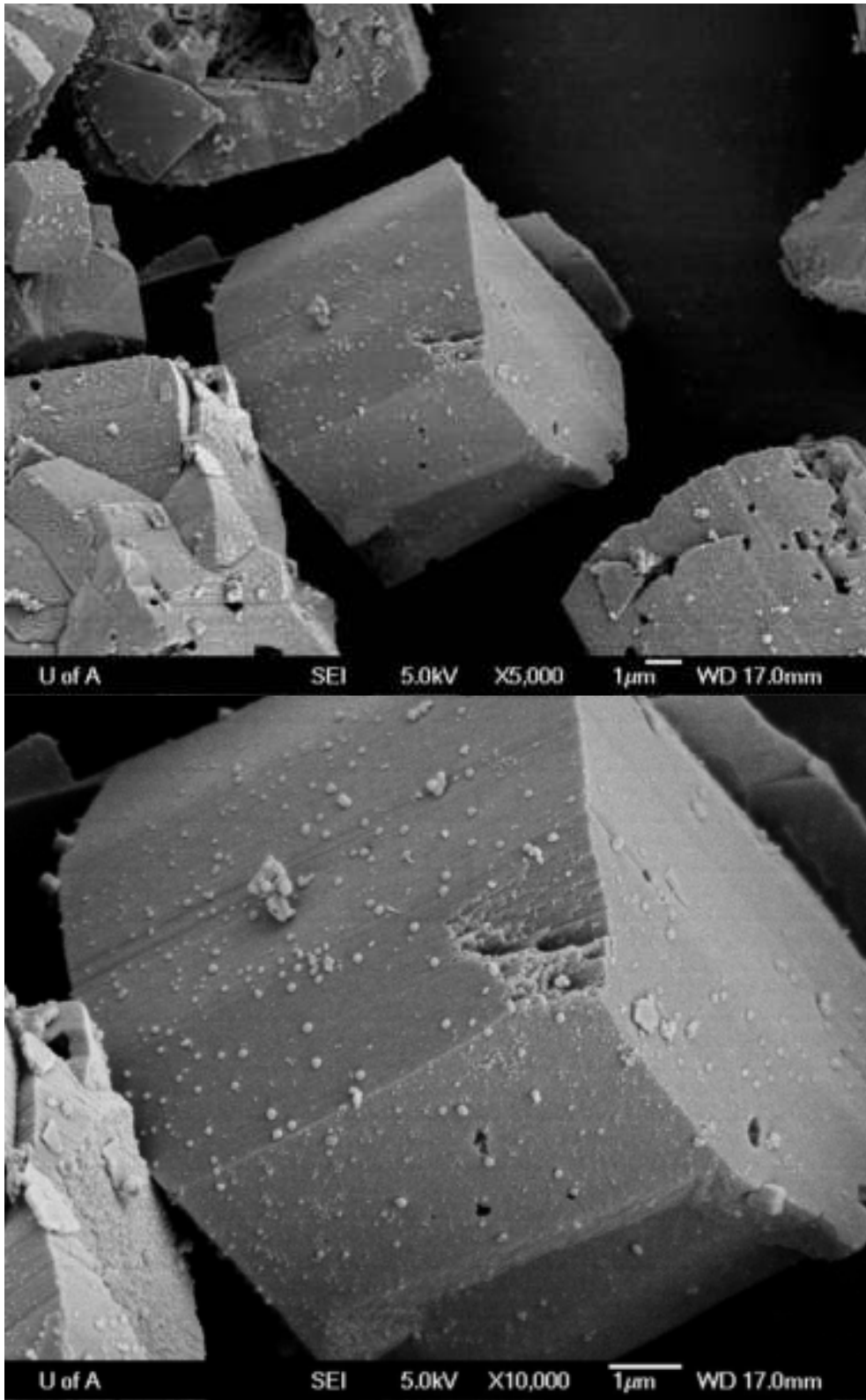
Figure 3.2 SEM images of Ag–ETS–10

Figure (3.3) illustrates AgCl fibres formed on the surface of ETS–10 crystals after the silver exclusion process.
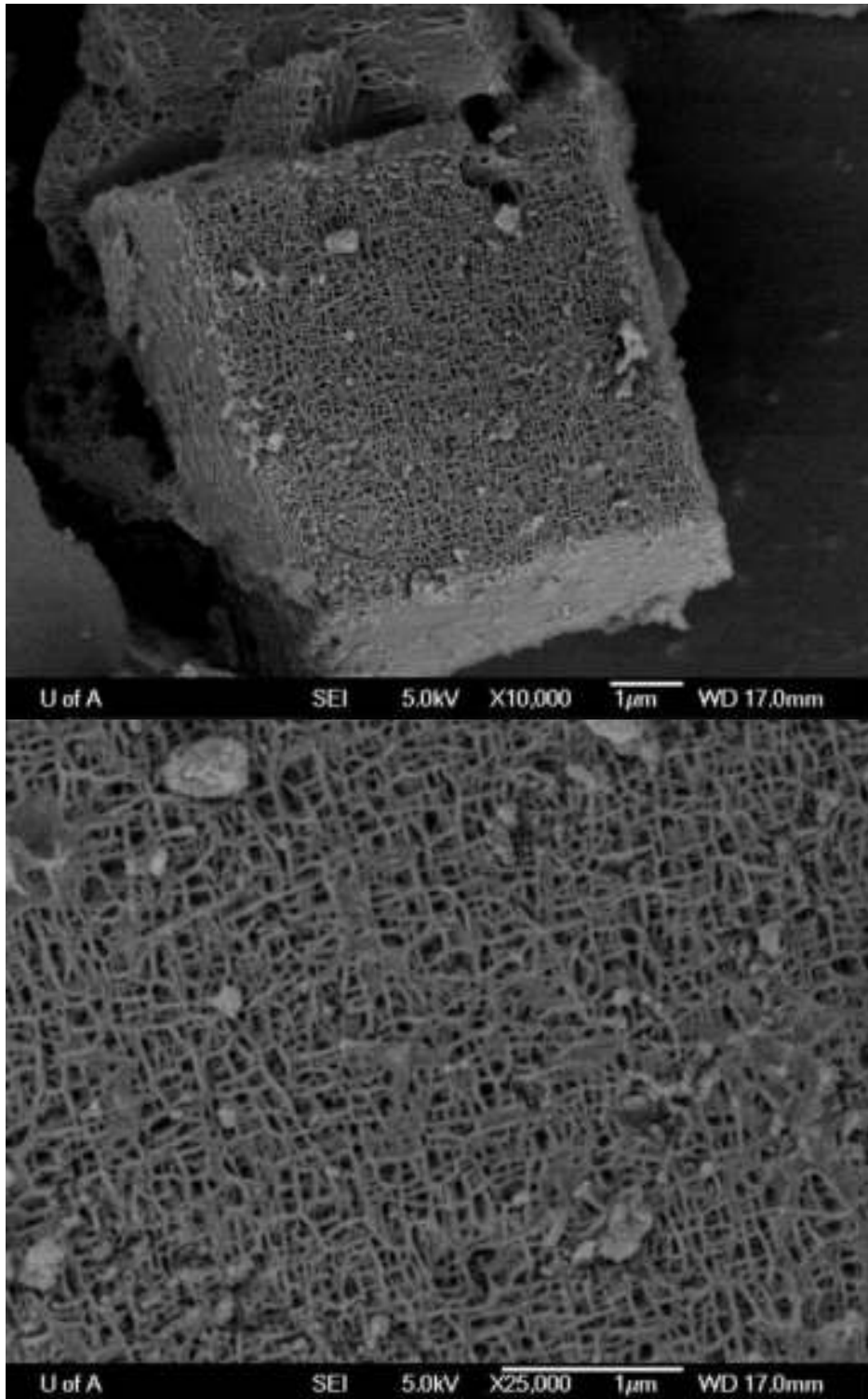
Figure 3.3 SEM images of AgCl fibres formed on ETS–10 crystals

EDX results of Ag–ETS–10 and AgCl–ETS–10 (after doing silver exclusion using highly concentrated $CaCl_2$ aqueous solution) showed that the ratio of silver to chloride in AgCl–ETS–10 sample is almost one, which means silver is completely bound by chloride and there is no free silver left. At this point the prominent ion inside the ETS–10 framework is Ca^{2+} and surface of the ETS–10 crystals is covered with silver chloride which is confirmed by the XRD data shown in Figure (3.4).
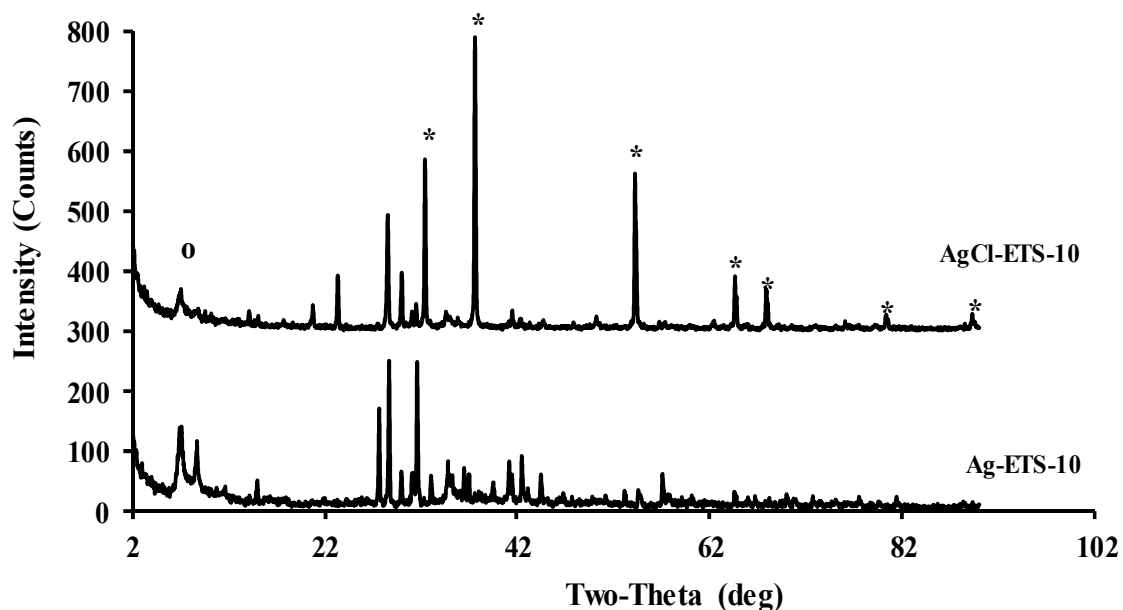
Figure 3.4 XRD patterns of Ag-ETS-10 and AgCl-ETS-10; asterisk and circle show peaks related to crystalline AgCl and ETS-10, respectively.

The XRD data demonstrate that ETS peak (marked with circle) is suppressed as silver chloride is formed on the surface and instead bigger peaks of crystalline silver chloride appear (marked with asterisk). Disappearing of the ETS–10 peaks is due to AgCl fibers growth on the surface, which prevents X-ray from reaching the ETS–10 crystals.

In order to investigate the influence of the free silver (silver which is not bound with Chloride) on the N_2/O_2 and Ar/O_2 selectivities, different concentrations of $CaCl_2$ were used for ion exchange with Ag–ETS–10. As a result, different amount of AgCl were formed on the ETS–10 surface which left various amounts of free active silver to participate in adsorption. Ag–ETS–10 was ion exchanged with the following $CaCl_2$ aqueous solutions: 5%, 10%, 20%, 30%, 50%, 70%, 90%, and 300% of ETS–10 cation exchange capacity (CEC). The results of XRD study of these samples are presented in the Figure (3.5). According to the XRD patterns, as the concentration of $CaCl_2$ in exchanging solution is increased from 5% to 50% of CEC, the intensity of the peaks corresponding to crystalline AgCl (which is asterisked in the XRD patterns) increased while the intensity of peak corresponding to ETS–10 decreased (which is marked with circle). For higher than 50% CEC, an increase in $CaCl_2$ concentration had no impact on the peak intensities indicating that all the silver present in Ag–ETS–10 is converted to AgCl and there is no more free silver left. The result is further verified with the data collected from inverse gas chromatography (IGC). Adsorption strength of each of the samples is tested in gas chromatography by injecting 1 ml of air, pure Ar and O_2 and a 50–50 vol.% mixture of Ar/O_2 at 303 K. Table (3.1) lists the atomic percent of Ag and Cl present in each of the samples exchanged with different amounts of $CaCl_2$ obtained from EDX data, the amount of calculated free Ag, and the selectives of N_2/O_2 and Ar/O_2 calculated from IGC results. According to the results in Table (3.1), the maximum selectivity value for Ag–ETS–10 is reached in the presence of maximum amount of free silver (no chloride). As the $CaCl_2$ concentration increases, the free active silver and consequently selectivities decrease. When there is no more free active silver left to react with Cl^-, the AgCl formation plateaus and the N_2/O_2 and Ar/O_2 selectivities remain unchanged.
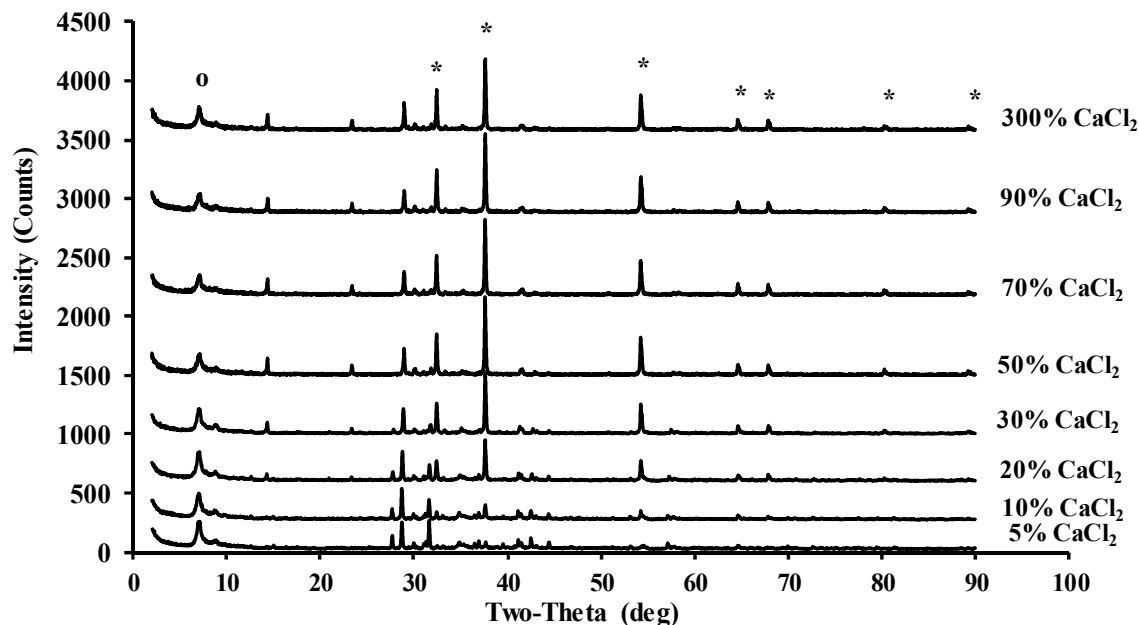
Figure 3.5 XRD patterns of samples washed with different amounts of $CaCl_2$ including: 5%, 10%, 20%, 30%, 50%, 70%, 90%, and 300% $CaCl_2$. Asterisk and circle marks correspond to peaks related to crystalline AgCl and ETS–10, respectively.

Table 3.1 The atomic percentage of silver, chloride, and free silver and N_2/O_2 and Ar/O_2 selectivities on adsorbents with different amounts of AgCl.

Sample Name	Ag (Atomic %)	Cl (Atomic %)	Free Ag* (Atomic %)	Selectivity (N_2/O_2)	Selectivity (Ar/O_2)
Ag–ETS–10	7.46	0	7.46	11.0	1.40
5% $CaCl_2$–Ag–ETS–10	7.19	1.16	6.03	8.7	1.3
10% $CaCl_2$–Ag–ETS–10	6.98	2.08	4.90	6.1	1.2
20% $CaCl_2$–Ag–ETS–10	7.39	3.32	4.08	2.3	1.1
30% $CaCl_2$–Ag–ETS–10	6.22	3.06	3.16	2.2	1.1
50% $CaCl_2$–Ag–ETS–10	4.24	3.97	0.27	2.1	1.0
70% $CaCl_2$–Ag–ETS–10	2.39	2.40	0.00	2.1	1.0
90% $CaCl_2$–Ag–ETS–10	2.72	2.70	0.00	2.1	1.0
300% $CaCl_2$–Ag–ETS–10	2.57	2.67	0.00	2.1	1.0

* Free Silver: The amount of silver isn't bound with chloride and is free to participate in the adsorption.

Figure (3.6) shows the inverse chromatographic profiles for air, Ar, O_2 and a 50–50% mixture of Ar/O_2 on Ag–ETS–10, Ag–ETS–10 washed with 5 %, 10 %, and 90 % $CaCl_2$ which are labelled as 5%$CaCl_2$–Ag–ETS–10, 10%$CaCl_2$–Ag–

ETS–10, and 90%CaCl$_2$–Ag–ETS–10, respectively. To perform the IGC, the helium carrier gas flow rate was 30 ml/min. As can be seen in the Figure (3.6), retention times of Ar, O$_2$ and N$_2$ decrease and the selectivities drop as the amount of AgCl formed on the ETS–10 increases while the concentration of free silvers decreases. In the case of mixed Ar-O$_2$, chromatographic splitting is much more obvious for Ag–ETS–10 than that of 5%CaCl$_2$–Ag–ETS–10 and 10%CaCl$_2$–Ag–ETS–10. Finally, as the amount of AgCl formed on ETS–10 increases to the point when there is no free silver left, there won't be any separation when Ar-O$_2$ mixture is injected, and both Ar and O$_2$ show the same affinity.
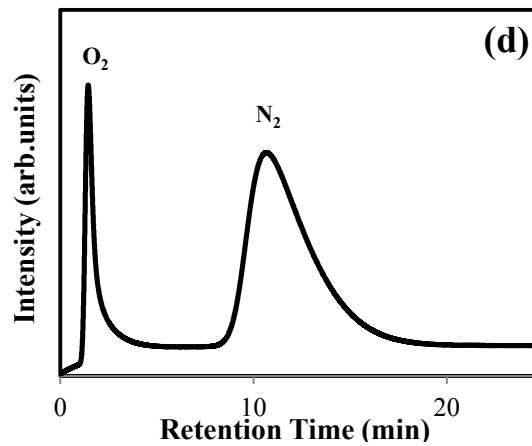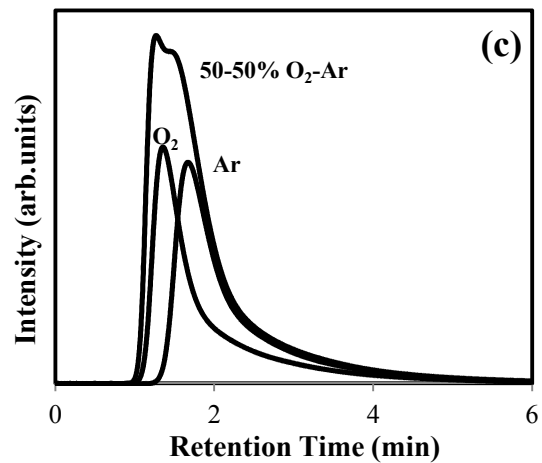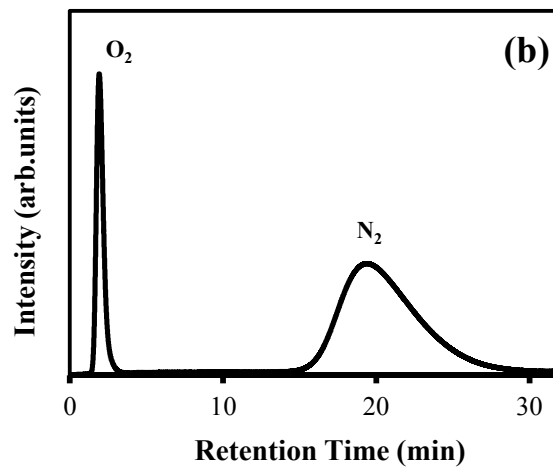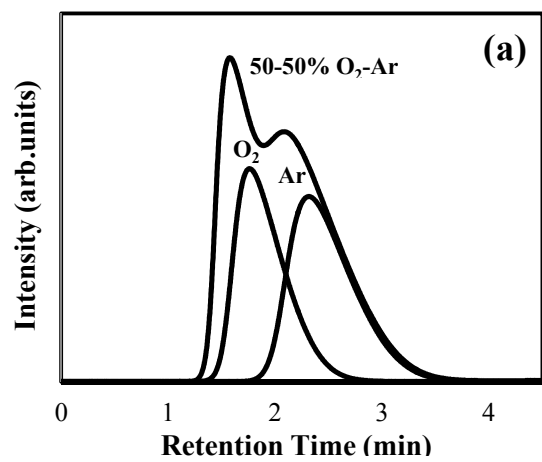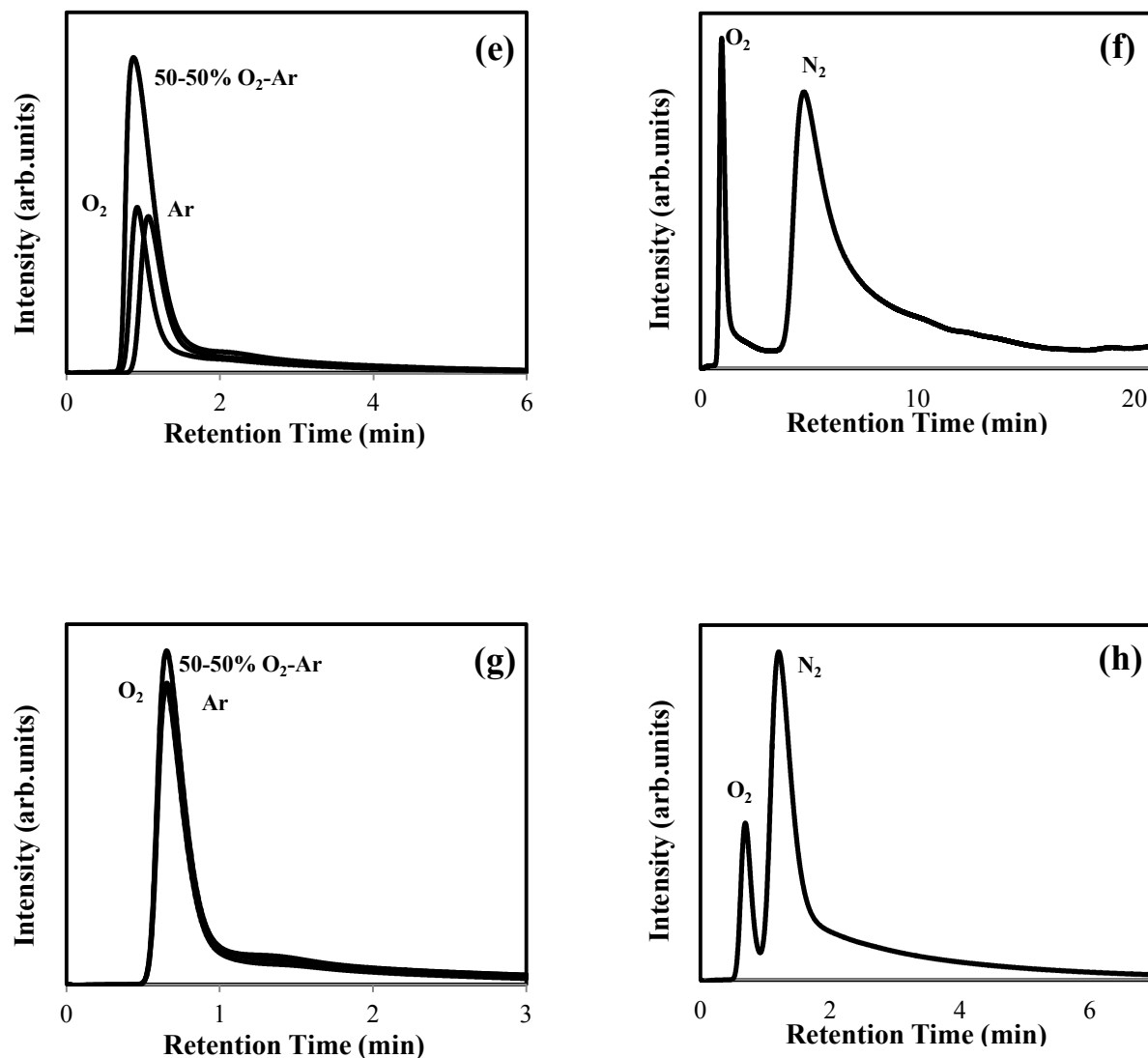
Figure 3.6 Gas chromatographic profiles obtained at 303 K with 30 ml/min helium carrier flow for Air, Ar, O$_2$ and a 50–50% mixture of Ar/O$_2$ on (a), (b) Ag–ETS–10; (c), (d) 5%CaCl$_2$–Ag–ETS–10; (e), (f) 10%CaCl$_2$–Ag–ETS–10; (g), (h) 90%CaCl$_2$–Ag–ETS–10.

3.4 Conclusions

Silver nanoparticles' influence on the air separation was studied using data collected from XRD, EDX analyses, and inverse gas chromatography (IGC). The adsorption selectivities of Ar/O_2 and N_2/O_2 calculated from IGC data show that Ag–ETS–10 had the highest selectivity values and the maximum amount of free active silvers (non-complex silvers). As the amount of free silver decreased, owing to the formation of the AgCl, a gradual decrease in the adsorption selectivities was observed. When the amount of $CaCl_2$ added to the exchanged solution reached 50% CEC or more, both the amount of AgCl formed and the selectivities reached a plateau. This is due to the removal of all the free silvers as they are bounded with chloride to form AgCl. At 50% CEC it appears there is no more free silver left.

References:

[1] Hao, E., Kelly, K. L., Hupp, J. T., 2002, "Synthesis of Silver Nanodisks using Polystyrene Mesospheres as Templates", Journal of the American Chemical Society, 124(51) pp. 15182-15183.

[2] Chen, S., Fan, Z., and Carroll, D. L., 2002, "Silver Nanodisks:â€‰ Synthesis, Characterization, and Self-Assembly", The Journal of Physical Chemistry B, 106(42) pp. 10777-10781.

[3] Maillard, M., Giorgio, S., and Pileni, M., 2002, "Silver Nanodisks", Advanced Materials, 14(15) pp. 1084-1086.

[4] Tan, Y., Li, Y., and Zhu, D., 2003, "Preparation of Silver Nanocrystals in the Presence of Aniline", Journal of Colloid and Interface Science, 258(2) pp. 244-251.

[5] Metraux, G.S., and Mirkin, C. A., 2005, "Rapid Thermal Synthesis of Silver Nanoprisms with Chemically Tailorable Thickness", Advanced Materials, 17(4) pp. 412-415.

[6] Jin, R., Cao, Y., Mirkin, C. A., 2001, "Photoinduced Conversion of Silver Nanospheres to Nanoprisms", Science, 294(5548) pp. 1901-1903.

[7] Callegari, A., Tonti, D., and Chergui, M., 2003, "Photochemically Grown Silver Nanoparticles with Wavelength-Controlled Size and Shape", Nano Letters, 3(11) pp. 1565-1568.

[8] Sun, Y., Mayers, B., and Xia, Y., 2003, "Transformation of Silver Nanospheres into Nanobelts and Triangular Nanoplates through a Thermal Process", Nano Letters, 3(5) pp. 675-679.

[9] Chen, S., and Carroll, D. L., 2004, "Silver Nanoplates: Size Control in Two Dimensions and Formation Mechanisms", The Journal of Physical Chemistry B, 108(18) pp. 5500-5506.

[10] Caswell, K. K., Bender, C. M., and Murphy, C. J., 2003, "Seedless, Surfactantless Wet Chemical Synthesis of Silver Nanowires", Nano Letters, 3(5) pp. 667-669.

[11] Sun, Y., Mayers, B., Herricks, T., 2003, "Polyol Synthesis of Uniform Silver Nanowires: A Plausible Growth Mechanism and the Supporting Evidence", Nano Letters, 3(7) pp. 955-960.

[12] Sun, Y., Gates, B., Mayers, B., 2002, "Crystalline Silver Nanowires by Soft Solution Processing", Nano Letters, 2(2) pp. 165-168.

[13] De, G., Licciulli, A., Massaro, C., 1996, "Silver Nanocrystals in Silica by Sol-Gel Processing", Journal of Non-Crystalline Solids, 194(3) pp. 225-234.

[14] Li, T., Moon, J., Morrone, A. A., 1999, "Preparation of Ag/SiO2 Nanosize Composites by a Reverse Micelle and Sol- Gel Technique", Langmuir, 15(13) pp. 4328-4334.

[15] Pérez-Robles, J. F., García-Rodríguez, F. J., Yáñez-Limón, J. M., 1999, "Characterization of sol–gel Glasses with Different Copper Concentrations Treated Under Oxidizing and Reducing Conditions", Journal of Physics and Chemistry of Solids, 60(10) pp. 1729-1736.

[16] Sun, Y., and Xia, Y., 2003, "Triangular Nanoplates of Silver: Synthesis, Characterization, and use as Sacrificial Templates for Generating Triangular Nanorings of Gold", Advanced Materials, 15(9) pp. 695-699.

[17] Chen, S., and Carroll, D. L., 2002, "Synthesis and Characterization of Truncated Triangular Silver Nanoplates", Nano Letters, 2(9) pp. 1003-1007.

[18] Zhou, Y., Wang, C. Y., Zhu, Y. R., 1999, "A Novel Ultraviolet Irradiation Technique for Shape-Controlled Synthesis of Gold Nanoparticles at Room Temperature", Chemistry of Materials, 11(9) pp. 2310-2312.

[19] Heilmann, A., Quinten, M., and Werner, J., 1998, "Optical Response of Thin Plasma-Polymer Films with Non-Spherical Silver Nanoparticles", The European Physical Journal B - Condensed Matter and Complex Systems, 3(4) pp. 455-461.

[20] Edmondson, M. J., Zhou, W., Sieber, S. A., 2001, "Electron-Beam Induced Growth of Bare Silver Nanowires from Zeolite Crystallites", Advanced Materials, 13(21) pp. 1608-1611.

[21] Li, C., and Wang, E., 2004, "Distribution and mRNA Expression of Î²-Catenin in Non-Small-Cell Lung Cancer", Chinese Journal of Lung Cancer, 7(1) pp. 27-30.

[22] Kuznicki, S., Kelly, D. J. A., Mitlin, D., 2010, "Mercury Adsorption using Chabazite Supported Metallic Nanodots", 12/518706(US Patent 2010/0050868 A1).

[23] Steven M., K., 2009, "Titanosilicate Molecular Sieve Supported Metallic Nanodots and Methods of use to Adsorb Noble Gases", 12/272366(US Patent 2009/0202655 A1).

[24] Tsapatsis, M., 2002, "Molecular Sieves in the Nanotechnology Era", AICHE Journal, 48(4) pp. 654-660.

[25] Gurin, V. S., Petranovskii, V. P., and Bogdanchikova, N. E., 2002, "Metal Clusters and Nanoparticles Assembled in Zeolites: An Example of Stable Materials with Controllable Particle Size", Materials Science and Engineering: C, 19(1-2) pp. 327-331.

[26] Gurin, V. S., Petranovskii, V. P., and Bogdanchikova, N. E., 2003, "Silver and Copper Nanostructures within the Erionite Regular Lattice: Interplay between Intra- and Extra-Crystalline Location", Materials Science and Engineering: C, 23(1-2) pp. 81-85.

[27] Gurin, V. S., Bogdanchikova, N. E., and Petranovskii, V. P., 2001, "Self-Assembling of Silver and Copper Small Clusters within the Zeolite Cavities: Prediction of Geometry", Materials Science and Engineering: C, 18(1-2) pp. 37-44.

[28] Gurin, V.S., and Petranovskii, V.P., 2004, "Studies in Surface Science and Catalysis",Elsevier, pp. 1661-1669.

[29] Gurin, V. S., Petranovskii, V. P., Hernandez, M., 2005, "Silver and Copper Clusters and Small Particles Stabilized within Nanoporous Silicate-Based Materials", Materials Science and Engineering A, 391(1-2) pp. 71-76.

[30] Kuznicki, S. M., Kelly, D. J. A., Bian, J., 2007, "Metal Nanodots Formed and Supported on Chabazite and Chabazite-Like Surfaces", Microporous and Mesoporous Materials, 103(1-3) pp. 309-315.

[31] Ansón, A., Kuznicki, S. M., Kuznicki, T., 2008, "Adsorption of Argon, Oxygen, and Nitrogen on Silver Exchanged ETS-10 Molecular Sieve", Microporous and Mesoporous Materials, 109(1-3) pp. 577-580.

[32] Kuznicki, and S. M., 1991, "Large-Pored Crystalline Titanium Molecular Sieve Zeolites", 07/348,226(US Patent 5011591).

[33] Ruthven, D.M., 1984, "Principles of Adsorption and Adsorption processes", John Wiley & Sons, Inc., Canada.

Chapter 4

The Potential of Pure Oxygen Production by

Ag–ETS–10

4.1 Introduction

Air separation is one of the most important gas separation processes in the world in which air is mostly being separated to its primary constituents including: nitrogen, oxygen, and argon. Two common techniques to carry out air separation are cryogenic distillation and adsorption. Cryogenic method is based on differences in the relative volatilities of the components and it is usually used to produce high amount of products with very high purity. Although this method is simple, it is very high energy intensive and involves many stages due to the closeness of boiling points. Although this purity of O_2 is appropriate for most industrial applications such as steel manufacturing, welding of metals, still higher purity of O_2 is required for some other applications. In addition, Ar recovery with high purity is significantly needed for applications such as welding, electrical appliances, and degassing in steel production. It is worth to mention that due to

very small amount of Ar in O_2, the best adsorbent for this purpose must be selective towards Ar [1-4].

Adsorptive processes such as Pressure Swing Adsorption (PSA) for air separation as an alternative for distillation processes are of high importance since they can significantly cut energy costs, but they are good for lower quantities and less pure products. In adsorption processes, one component preferentially adsorbs, therefore choosing the right adsorbent with the appropriate extra framework cations as the active sites play the most important role [4-7]. By the way, it has been demonstrated that density and location of the cations in the zeolite structure has a huge influence on gas adsorption and also heat of adsorption [8].

Since nitrogen molecule has a larger quadrupole moment (5.0035×10^{-40} cm^3) than that of oxygen (0.800×10^{-40} cm^3) it is able to adsorb stronger on molecular sieves. This is reflected in its higher heat of adsorption [1, 9, 10]. Hence, splitting air to N_2 and O_2 could be done simply on so many proposed molecular sieve adsorbents. Unlike N_2/O_2 separation, the adsorption separation of a mixture of Ar/O_2 is very challenging owing to similar physical properties of both species [11-15].

PSA processes have been tremendously employed commercially in the past several decades [16]. Many research efforts have been carried out using kinetically controlled PSA by developing adsorbents which preferentially adsorbs O_2 rather than Ar [1, 4]. Rege et al. employed a couple of pressure swing adsorption (PSA) units to produce high purity (> 99%) oxygen and argon from a mixture of 95% O_2–5% Ar using carbon molecular sieve (CMS) as the adsorbent [1]. It has been suggested that by taking advantage of using two–stage PSA process with two different adsorbent, high purity O_2 can be produced. In this process, oxygen product was 99% pure with 50% recovery and in the first step CMS was exploited to remove Ar and Ca–X zeolite in the second stage for N_2 removal from a N_2/O_2 mixture [17]. A series of inverse gas chromatographic experiments has been performed to determine the high resolution and high ability of calcium, lithium, and potassium chabazites to selectively adsorb oxygen from a

mixture of Ar/O_2 [8, 18]. O_2 and Ar adsorption is not only due to the electrostatic interaction of these molecules with lattice atoms but also with extra-framework cations. Thus, a slight quadrupole moment of O_2 provides a larger interaction with cations, i.e., larger heat of adsorption in comparison to Ar (without any quadrupole moment).

It has been reported that silver–mordenite has some adsorption preference towards Ar rather than O_2 and the higher the silver loading, the higher the selectivity. However, other cation–exchanged mordenite sorbents didn't show any selectivity [19]. It has been also reported that silver–exchanged zeolites A, X, Y, mordenite, BEA, L, and ZSM–5 exhibit argon selectivity to a certain extent. It is believed that silver–exchanged zeolites have stronger interaction with nitrogen molecules than that of other counterpart cation–exchanged zeolites which results in higher selectivity and higher adsorption capacity [5, 20]. While, Ag–X is argon selective, Co–X preferentially adsorbs O_2 [15].

Silver as a transition metal has a strong impact on zeolites and silver–exchanged molecular sieves reveal puzzling adsorption behavior. It is believed that this can be related to d–orbitals in silver ion which give it directional properties that cannot be seen in closed shell alkaline and alkaline earth–exchanged zeolites [10, 21, 22]. Therefore, silver–exchanged molecular sieves not only show much stronger interaction with N_2, but also an increase in Ar adsorption can be seen [5, 10, 20]. Stronger interaction of N_2 molecules with silver ions in the silver exchanged–molecular sieves has been explained through π–complexation mechanism which for the first time was put forth by Dewar (1950). According to this theory, two phenomena happen: formation of a σ bond owing to the donation of the π electrons from N_2 to the empty 5s orbital of Ag^+, and at the same time, back–donation of the 4d electrons (filled with 10 electrons) of Ag^+ to the empty antibonding π orbitals of N_2 which results in the formation of a weak π–complexation and consequently in very high values for heat of adsorption, adsorption selectivity, and Henry's constant. Unlike N_2, O_2 has partially filled antibonding π orbitals which prevent 4d electrons of Ag^+ from back–donation and consequently formation of weak π–complexation [5, 6]. Nobel

65

gases also interact strongly with silver. This strength decreases significantly in the order Xe > Kr > Ar, but still there is a significant affinity between silver and Ar [23]. This strong sorption affinity of Ar on silver–exchanged zeolites is due to the formation of the Ar(p π)–Ag(d π) bonding molecular orbital to transfer electrons [5].

ETS–10 is a microporous mixed coordinated titanosilicate molecular sieve in which orthogonal TiO_6 and tetrahedral SiO_4 are tetrahedrally linked to oxygen atoms. Since each titanium carries two negative charges, it requires two monovalnet cations to remain neutral and is usually balanced by Na^+ and K^+ [24, 25]. It has been discovered that Ag–ETS–10 has a strong potential to selectively adsorb noble gas Xenon [26].

In this study, the potential of silver–exchanged ETS–10 in order to produce high purity O_2 (>99%) was investigated. Single adsorption isotherms were evaluated for N_2, O_2 and Ar. The corresponding binary mixtures were predicted using IAST model.

4.2 Experimental Methods

Materials. ETS–10 was synthesized as explained in the third chapter section (3.2).

Silver Exchange. In order to prepare silver exchanged ETS–10, as synthesized Na–ETS–10 powder was exposed to an excess of aqueous solution of $AgNO_3$ (obtained from Fisher) at 353 K stirring for 1 hour. The ratio used for silver exchange was 1:1:10 which refers to amounts of Na–ETS–10, $AgNO_3$, and de-ionized water, respectively. This process was repeated for three times to ensure that it is fully exchanged. The exchanged materials were thoroughly washed and vacuum filtered with de-ionized water after each exchange and finally dried in the oven at 353 K.

X-ray powder diffraction (XRD) and scanning electron microscopy (SEM) tests and inverse gas chromatographic measurements (IGC) were performed as explained in chapter 3 section (3.2).

Equilibrium Adsorption Isotherm Measurements. Adsorption isotherms were measured volumetrically at 298 K up to 100 kPa using an AUTOSORB–1–MP from Quantachrome Instruments (Boynton Beach, FL) on crystalline powders (no binders or diluents were added to the samples). Adsorption isotherms at higher pressures (up to 500 kPa) were measured at 298 K with an HPVA-100 High Pressure Volumetric Analyzer adsorption unit from VTI instruments (Hialeah, FL). All samples were activated at 523 K for 10 h under vacuum ($<5 \times 10^{-4}$ Torr).

Experimental data were fitted to classical Langmuir equation:

$$q_i = \frac{q_{i,m} \cdot b_i \cdot P_i}{1 + b_i \cdot P_i} \tag{4-1}$$

Where q_i is the amount adsorbed (mmol/g) at the pressure P (kPa), and b_i is the Langmuir equilibrium constant. $q_{i,m}$ is the maximum adsorption capacity (mmol/g), At low loading, as pressure approaches zero, the Henry's low constant can be obtained as $K_i = q_{i,m} \cdot b_i$ (mmol g^{-1} kPa^{-1}). The Henry selectivity (α) was calculated as:

$$\alpha(i/j) = \frac{K_i}{K_j} \tag{4-2}$$

Where, $\alpha_{i/j}$ stands for the selectivity of component i over j. The Ideal Adsorbed Solution Theory (IAST) developed by Myers and Prautnitz (1965) was used to estimate binary isotherms based on single component data. The equilibrium selectivity $S_{i/j}$ is defined as:

$$S_{i/j} = \frac{X_{i/}X_j}{Y_{i/}Y_j} \tag{4-3}$$

In which, *X,* and *Y* are the mole fraction in the adsorbed and gas phase, respectively.

4.3 Results and Discussion

It was observed that Ag–ETS–10 sample's color changed after activation at 473 K in vacuum, from light brown to dark gray. Many researches have been confirmed that as silver–zeolite is being heated, silver clusters with different sizes and compositions form in different sites in the zeolites. These clusters may be neutral or charged. Depending upon cluster's locations and compositions, silver–zeolites exhibit various colors such as white, pale yellow, dark gray and so on [5, 20-22, 27].

XRD patterns of silver–exchanged–ETS–10 was compared with that of untreated as–synthesized ETS–10 materials and confirmed that the crystalline structure of the sample was retained after several consecutive silver exchanges. In addition, SEM images of both as–synthesized ETS–10 and Ag–ETS–10 verified that cubic morphology and crystal size were remained unchanged after silver exchange.

Results achieved from inverse gas chromatograph for air, pure Ar, O_2, and a 50–50% mixture of Ar/O_2 at 303 K are shown in Figure (4.1). As observed in Figure (4.1.a), Ar takes longer time to elute from the column in comparison to O_2. Thus, a longer retention time for Ar is reflecting a stronger affinity to Ag–ETS–10. The selectivites calculated from equation (3-1) in the third chapter for Ar/O_2 and N_2/O_2 are: 1.4 and 11.5, respectively.

Low pressure adsorption isotherms for Ar, O_2, and N_2 on Ag–ETS–10 at 298 K along with their Langmuir isotherm fitting curves are depicted in Figure (4.2). Langmuir model was the best fit for all the adsorption isotherms. The parameters of Langmuir isotherms are tabulated in Table (4.1). These parameters were used to predict Henry's constants as well as the corresponding N_2/O_2 and Ar/O_2 selectivities. Ag–ETS–10 shows high N_2/O_2 selectivity of 13.05 and Ar/O_2 selectivity approaches 1.41 at very low pressures at Henry's law limiting region. The Henry's selectivities obtained from equilibrium adsorption isotherms at 298 K are consistent with selectivities calculated using IGC data at 303 K. These

values are much higher than that of reported by other researchers for silver–exchanged zeolites A, X, Y, L, BEA, mordenite, and ZSM–5 [5, 6].
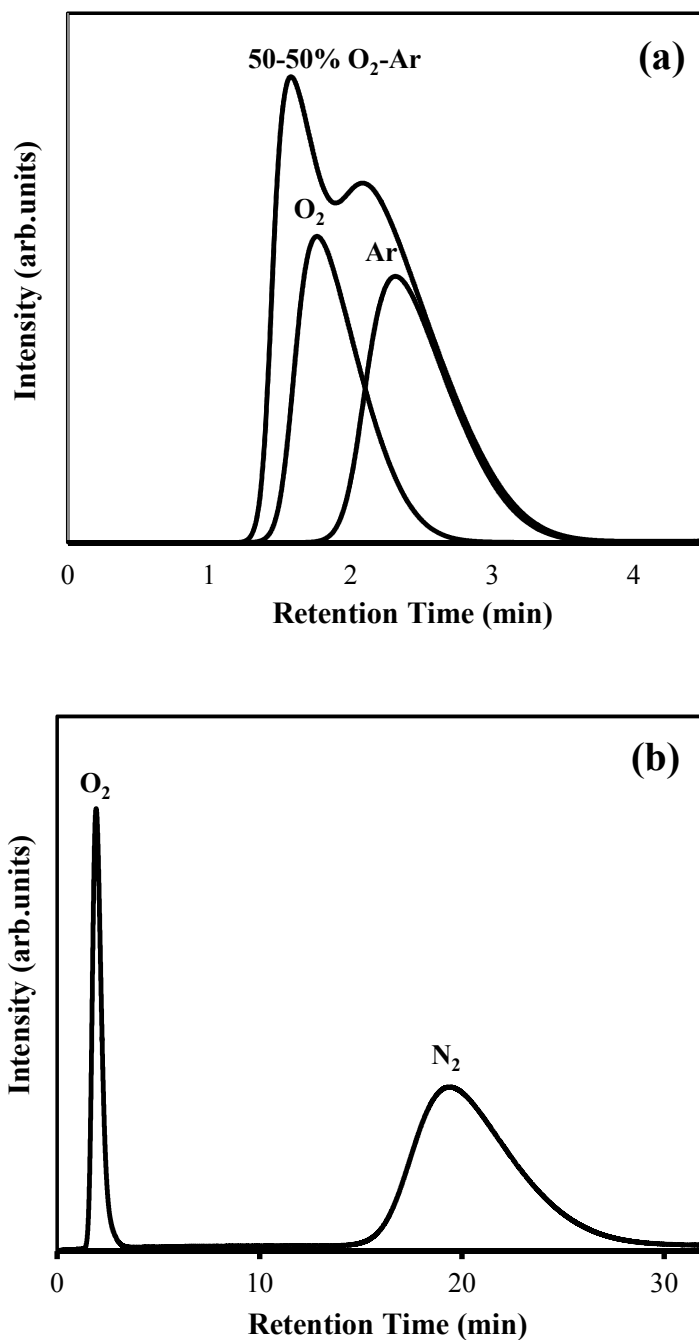
Figure 4.1 Gas chromatographic profiles obtained at 303 K with 30 ml/min helium carrier gas for (a) pure O_2, Ar, and 50–50% mixture of Ar/O_2, (b) Air on Ag–ETS–10
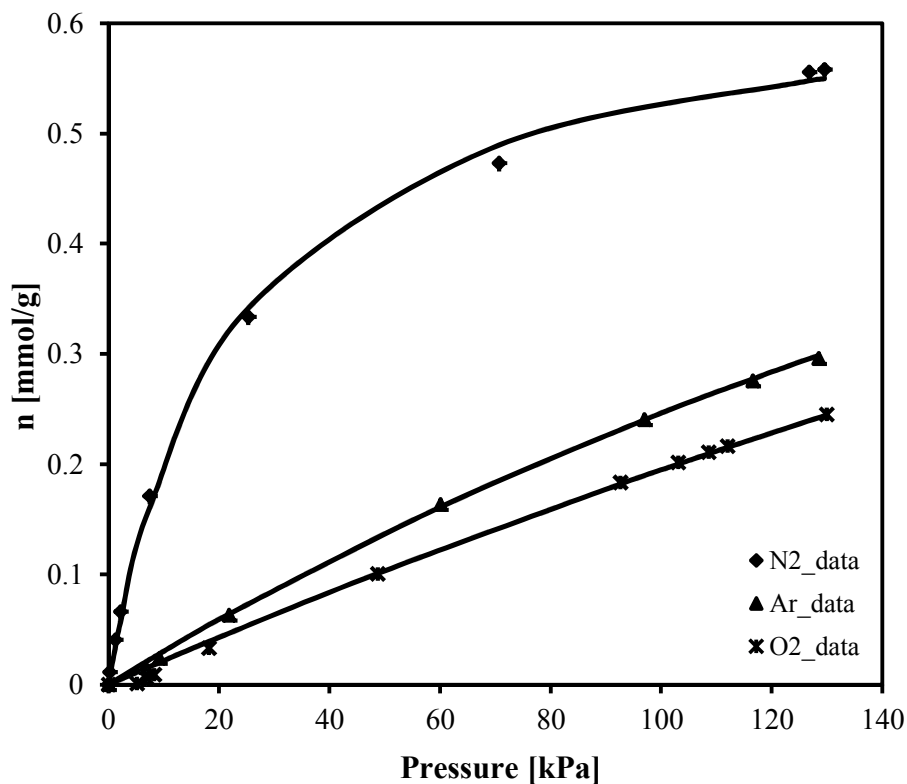
Figure 4.2 Low Pressure Isotherms for N_2, O_2, and Ar on Ag–ETS–10 at 298 K and Langmuir model curve fitted for each data

Table 4.1 Henry's law constants (K_i), maximum adsorption capacities (q_m), and N_2/O_2 and Ar/O_2 ideal selectivities for low pressure adsorption isotherms on Ag–ETS–10

Langmuir Parameters (0–120 kPa)		Ag–ETS–10
Nitrogen	$K_i \cdot 10^3$ (mmol kPa^{-1} g^{-1})	28.7
	q_m (mmol g^{-1})	0.645
	b_i (kPa^{-1})	0.045
Argon	$K_i \cdot 10^3$ (mmol kPa^{-1} g^{-1})	3.1
	q_m (mmol g^{-1})	1.172
	b_i (kPa^{-1})	0.003
Oxygen	$K_i \cdot 10^3$ (mmol kPa^{-1} g^{-1})	2.2
	q_m (mmol g^{-1})	1.686
	b_i (kPa^{-1})	0.001
	α (N_2/O_2)	13.05
	α (Ar/O_2)	1.41
	α (N_2/Ar)	9.26

High pressure adsorption isotherms for Ar, O_2, and N_2 along with their Langmuir fitting curves at 298 K on Ag–ETS–10 are shown in Figure (4.3). The Langmuir parameters are listed in the Table (4.2).
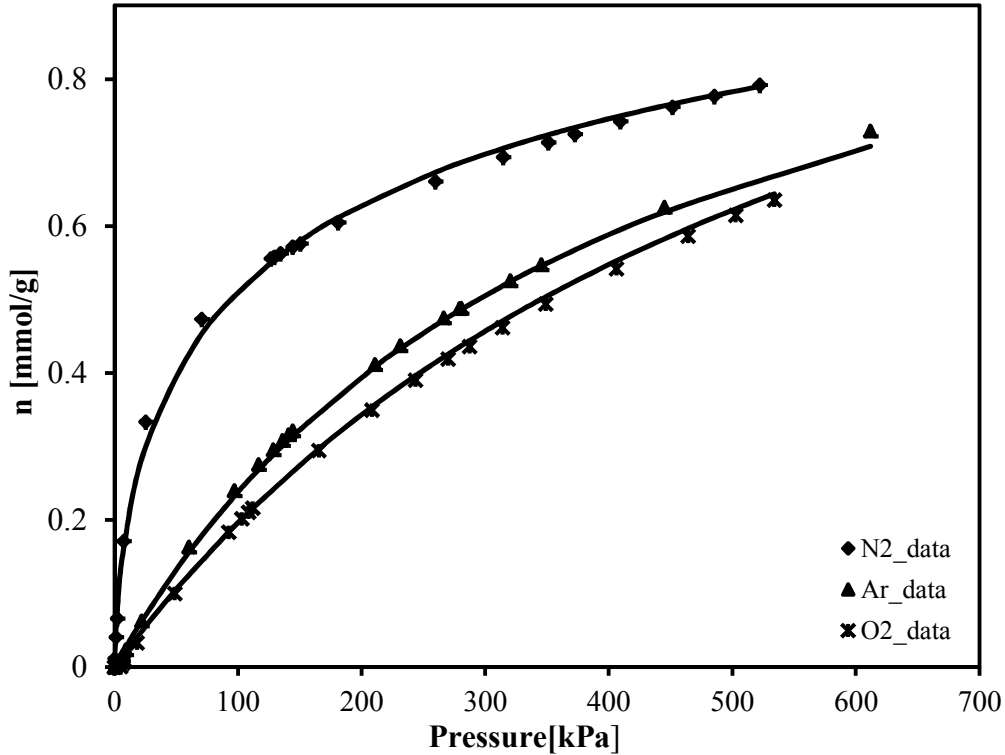
Figure 4.3 High Pressure Isotherms for N_2, O_2, and Ar on Ag–ETS–10 at 298 K

Table 4.2. Langmuir adsorption parameters for N_2, Ar, and O_2 for high pressure (0–500 kPa) isotherms on Ag–ETS–10

Langmuir (0–500 kPa)		AgETS–10
Nitrogen	$b_i \cdot 10^2 \, (kPa^{-1})$	1.87
	$q_m \, (mmol \, g^{-1})$	0.82
Argon	$b_i \cdot 10^2 \, (kPa^{-1})$	0.26
	$q_m \, (mmol \, g^{-1})$	1.17
Oxygen	$b_i \cdot 10^2 \, (kPa^{-1})$	0.17
	$q_m \, (mmol \, g^{-1})$	1.32

Figure (4.4) depicts IAST model predictions of the equilibrium adsorption selectivities of N_2/O_2 and Ar/O_2 as a function of total pressure at 298 K for binary gaseous mixtures of ($y_{N2} = 0.79$, $y_{O2} = 0.21$) and ($y_{Ar} = 0.05$, $y_{O2} = 0.95$), respectively. The predicted N_2/O_2 selectivity decreases as the total pressure

71

increases. At lower pressures, Ag^+ tends to interact more strongly with N_2 than with O_2. So, N_2 adsorbs strongly to the adsorption sites due to its larger quadrupole moment compared to that of O_2. Therefore, at low pressures, N_2/O_2 selectivity is significantly high. However, as pressure increases, IAST mixture model estimations suggest that the amount of adsorbed N_2 would increase relatively less than O_2. On the other hand, in the case of Ar/O_2 selectivity at different total pressures, it almost remains constant. Due to weak quadrupole moment of O_2 (0.800×10^{-40} cm^3) and zero quadrupole moment of Ar, they almost adsorb in a similar manner. As a result, change in the pressure has the same effect on Ar and O_2 adsorption which means selectivity doesn't diminish so much at high pressures.
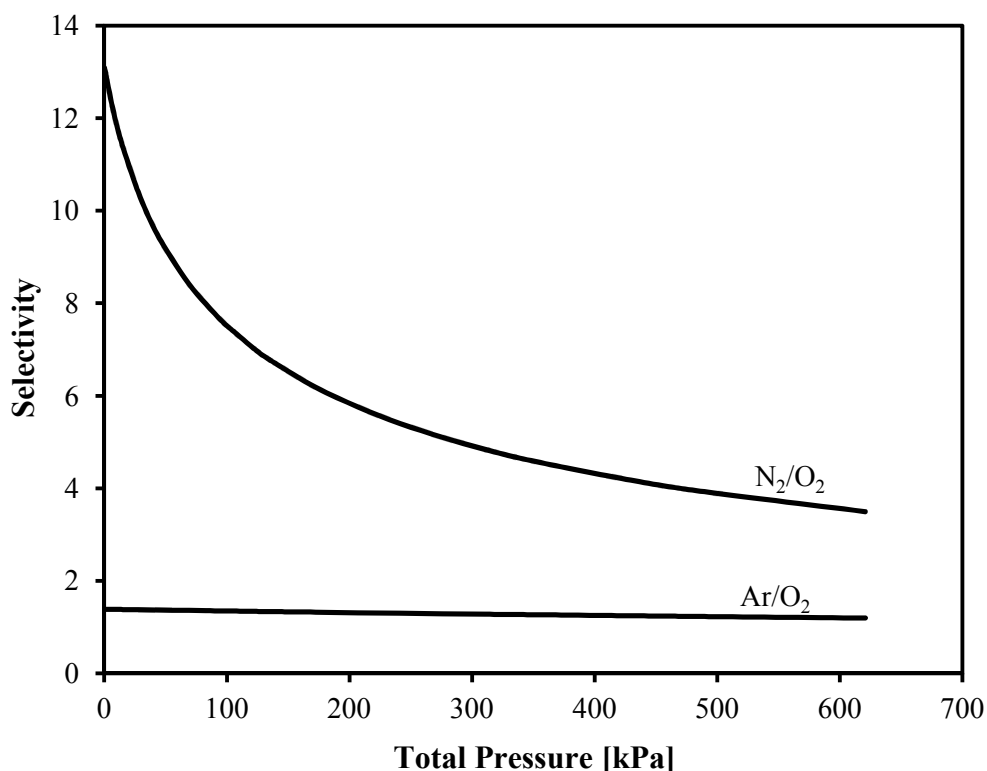
Figure 4.4 N_2/O_2 and Ar/O_2 selectivities on Ag–ETS–10 at 298 K for N_2 and Ar molar fraction in gas phase of 0.79 and 0.05, respectively

Applying IAS theory, N_2/O_2 equilibrium selectivity is plotted as a function of gas phase N_2 mole fraction (y_{N2}) at several different total bed pressures (Figure (4.5)). N_2/O_2 selectivity decreases as the gas composition is richer in N_2.

For a given value of y_{N2}, N_2/O_2 selectivity drops as total pressure of the bed increases as already shown in Figure (4.4).

Figure (4.6) depicts Ar/O_2 selectivity as a function of Ar mole fraction in the gas phase at four different total pressures. The dependency of Ar/O_2 selectivity on both pressure and gas composition is weak. Ar and O_2 adsorb similarly since both molecules have similar adsorption affinities and kinetics diameters. As a result, Ar/O_2 selectivity decreases slightly as pressure and Ar gas composition increase.

The same trends for N_2/O_2 and Ar/O_2 binary mixture selectivities as a function of pressure have been reported for several different silver exchanged zeolites including, zeolite A, X, Y, L, BEA, mordenite, and ZSM–5 [5, 6].
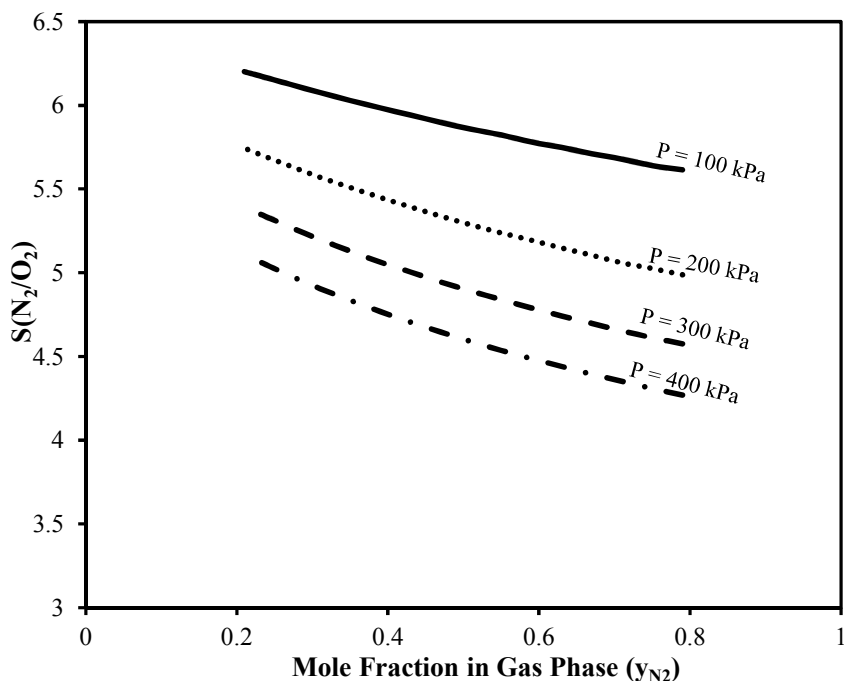
Figure 4.5 N_2/O_2 selectivity on Ag–ETS–10 as a function of N_2 mole fraction in the gas phase at 298 K at different total pressures
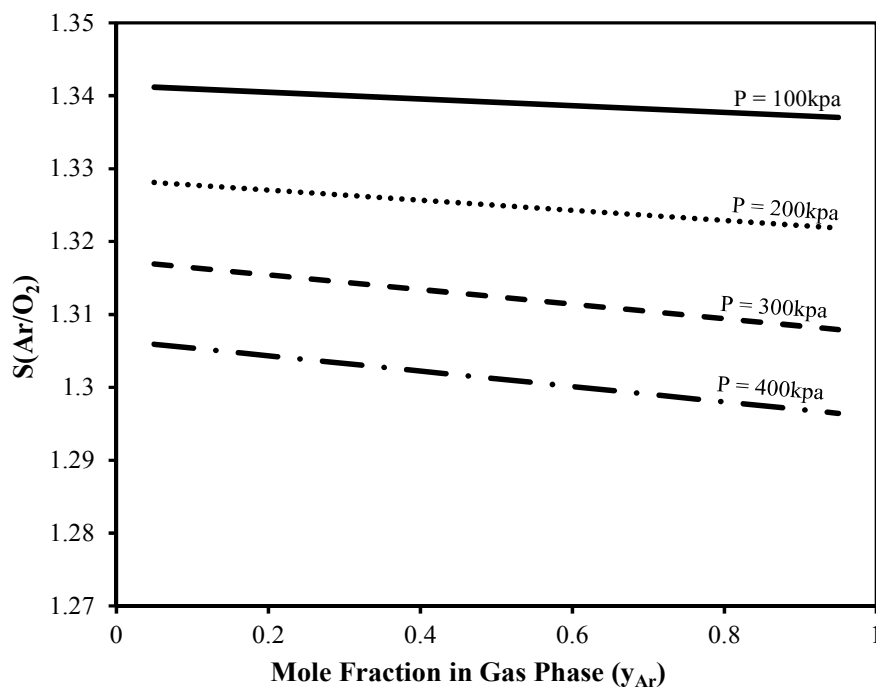
Figure 4.6 Ar/O$_2$ selectivity on Ag–ETS–10 as a function of Ar mole fraction in gas phase at 298 K at different total pressures

Due to the fact that Ar is present at very low concentrations in O$_2$ streams, relatively high selectivity for Ar is required to obtain high purity O$_2$. Ag–ETS–10 molecular sieve has this principal advantage with its unique structure and capabilities. Knaebel et al. reported that taking advantage of Ag–mordenite, O$_2$ can be produced with the purity of about 99.7% in the PSA unit [19, 23]. Ar/O$_2$ selectivity for Ag–ETS–10 obtained in the current study is 1.41 as shown in the Table (4.1), while it is reported 1.25 for Ag–mordenite [19, 23]. Furthermore, Ag–ETS–10 has higher bulk density than Ag–mordenite. Therefore, it can be concluded that Ag–ETS–10 is capable of producing higher purity O$_2$ stream compared to Ag–mordenite.

Pure Oxygen from an Air Stream. Pure O$_2$ from air could be recovered by using a single step adsorption column. The first layer inside the column would be mostly the zone for N$_2$/O$_2$ separation, while the remaining adsorbing layer would polish Ar from O$_2$. Thus, the second layer requires an adsorbent with selectivity

towards Ar over O_2. The first layer only requires selectivity towards N_2 over Ar and O_2. Therefore, Ag–ETS–10 is the strong candidate which shows both selectivity towards N_2 and Ar. Figure (4.7) depicts qualitatively the concentration changes in the gas stream at the different sectors. The feed is an air stream (N_2:79%; O_2:20%; Ar:1%) that passes into a first adsorption zone providing an intermediate stream with null (N_2:0%; O_2:95%; Ar:5%) or reduced N_2 content. In the second adsorption zone, Ar is mostly adsorbed together with any remaining N_2 content in the intermediate stream. An O_2–enriched gas (O_2:97–100%) can be obtained as a product or raffinate stream.
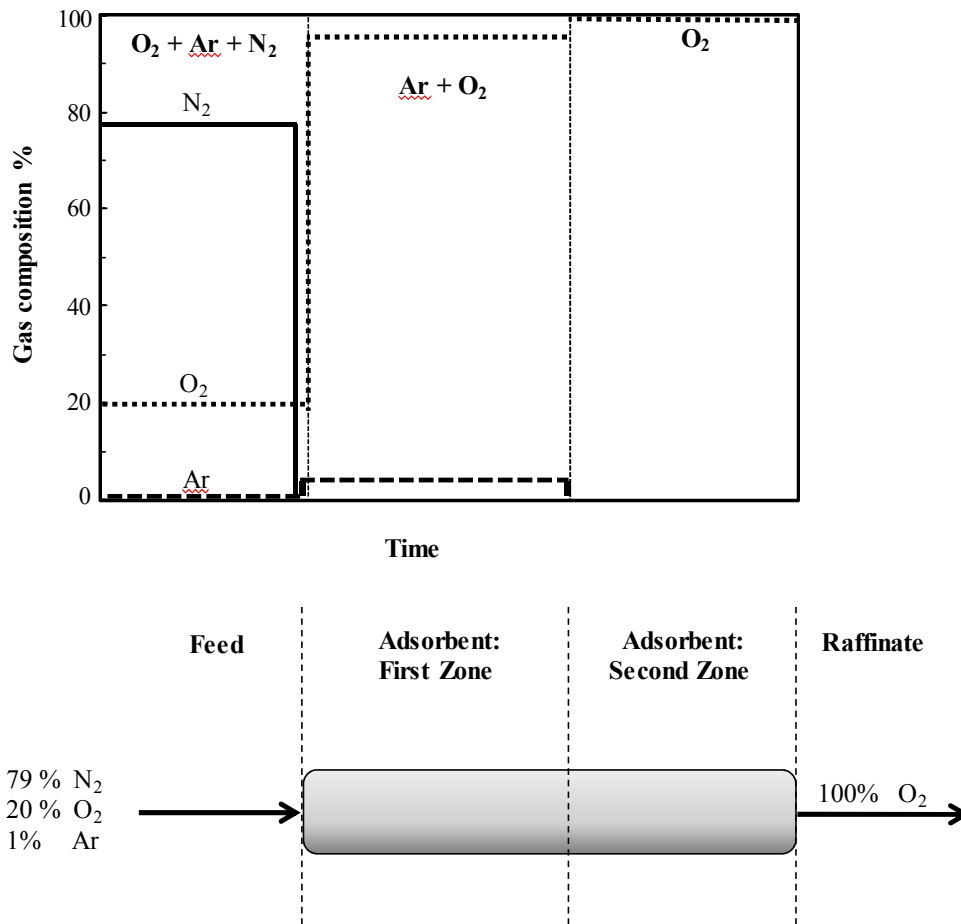

Figure 4.7 Pure O_2 from air using Ag–ETS–10 adsorbent: schematic of a single step adsorption column showing N_2, O_2, and Ar gas phase compositions on feed, adsorption column and raffinate.

Theoretical or ideal O_2 recoveries (single step column) in each zone using Ag–ETS–10 are shown in Table (4.3).

Table 4.3 Theoretical O_2 recoveries in the raffinate stream using
a single adsorption column with Ag–ETS–10

Separation Zone	Feed Composition			Column Pressure	O_2 Stream	
	N_2 (%)	O_2 (%)	Ar (%)	(kPa)	Purity (%)	Recovery (%)
N₂/(O₂+Ar)	79	20	1	100	95	68.7
				200	95	63.7
				300	95	59.6
Ar/O₂	0	95	5	100	100	9.6
				200	100	8.5
				300	100	7.5

The recovery values were estimated by means of mass balances using binary equilibrium adsorbed amounts predicted by IAST model. The O_2 recoveries are defined as the amount of O_2 obtained in the raffinate stream related to the O_2 content in the air feed. The O_2 recovery values are higher at lower pressures. At 100 kPa, the O_2 recovery for a 95% purity stream is ~69%. A 100% O_2 stream can be obtained with a theoretical recovery of ~10%. With this same approach, estimations suggest that the pure O_2 recovery is able to increase up to 22% by just improving Ar/O_2 selectivity from 1.4 up to 1.7.

4.4 Conclusions

The evaluation of adsorptive properties of Ag–ETS–10 including IGC and isotherms data demonstrate significantly high selectivity for N_2 over O_2 and a reasonable selectivity value for Ar over O_2 within a wide range of pressures. While N_2/O_2 selectivity tends to decrease as bed total pressure increases, Ar/O_2 selectivity is almost constant. The values of N_2/O_2 and Ar/O_2 selectivities at Henry's region are 13.05 and 1.41, respectively.

By taking advantage of Ag–ETS–10 in a PSA unit, high purity O_2 can be produced. By passing air through the Ag–ETS–10 bed at total pressure of 100

kPa, 68.7% O_2 with a purity of 95% can be recovered based on IAST model predictions. Moreover, pure O_2 with a recovery of 9.6% can be obtained in a single adsorption column packed with Ag–ETS–10. However, higher O_2 recovery values are expected based on material improvements and taking full advantage of the state of art PSA technology.

References:

[1] Rege, S. U., and Yang, R. T., 2000, "Kinetic Separation of Oxygen and Argon using Molecular Sieve Carbon", Adsorption, 6(1) pp. 15-22.

[2] Cabau, I. S., October 2005, "Improvement of the Properties of Zeolites for Application in the Nitrogen and Oxygen Separation Process and in Acid Catalysis", Thesis.

[3] Häring, H., February 2008, "industrial gases processing," Wiley-VCH, Weinheim Germany.

[4] Jin, X., Malek, A., and Farooq, S., 2006, "Production of Argon from an Oxygen and Argon Mixture by Pressure Swing Adsorption", Industrial & Engineering Chemistry Research, 45(16) pp. 5775-5787.

[5] Sebastian, J., and Jasra, R. V., 2005, "Sorption of Nitrogen, Oxygen, and Argon in Silver-Exchanged Zeolites", Industrial & Engineering Chemistry Research, 44(21) pp. 8014-8024.

[6] Yang, R. T., Chen, Y. D., Peck, J. D., 1996, "Zeolites Containing Mixed Cations for Air Separation by Weak Chemisorption-Assisted Adsorption", Industrial & Engineering Chemistry Research, 35(9) pp. 3093-3099.

[7] Jasra, R. V., Choudary, N. V., and Bhat, S. G. T., 1996, "Correlation of Sorption Behavior of Nitrogen, Oxygen, and Argon with Cation Locations in Zeolite X", Industrial & Engineering Chemistry Research, 35(11) pp. 4221-4229.

[8] Singh, R. K., and Webley, P., 2005, "Adsorption of N2, O2, and Ar in Potassium Chabazite", Adsorption, 11(0) pp. 173-177.

[9] Moon, I., Lee, D.,II, Yang, J., 1986, "Air Separation by Adsorption on Molecular Sieve 5A", Korean Journal of Chemical Engineering, 3(1) pp. 15-21.

[10] H. W. Habgood, 1964, "Adsorptive and Gas Chromatographic Properties of Various Cationic Forms of Zeolite X", Canadian Journal of Chemistry, 42pp. 2340.

[11] Peter, S. A., Moharir, A. S., and Jasra, R. V., 2010, "Selective Adsorption of Oxygen Over Argon in Alkaline-Earth-Metal Cation-Exchanged Zeolite X", Industrial & Engineering Chemistry Research, 49(16) pp. 7524-7529.

[12] Pillai, R. S., Peter, S. A., and Jasra, R. V., 2008, "Adsorption of Carbon Dioxide, Methane, Nitrogen, Oxygen and Argon in NaETS-4", Microporous and Mesoporous Materials, 113(1-3) pp. 268-276.

[13] Sebastian, J., Pillai, R. S., Peter, S. A., 2007, "Sorption of N2, O2, and Ar in Mn(II)-Exchanged Zeolites A and X using Volumetric Measurements and Grand Canonical Monte Carlo Simulation", Industrial & Engineering Chemistry Research, 46(19) pp. 6293-6302.

[14] Peter, S. A., Sebastian, J., and Jasra, R. V., 2005, "Adsorption of Nitrogen, Oxygen, and Argon in Mono-, Di-, and Trivalent Cation-Exchanged Zeolite Mordenite", Industrial & Engineering Chemistry Research, 44(17) pp. 6856-6864.

[15] Sebastian, J., Peter, S. A., and Jasra, R. V., 2005, "Adsorption of Nitrogen, Oxygen, and Argon in Cobalt(II)-Exchanged Zeolite X", Langmuir, 21(24) pp. 11220-11225.

[16] Ralph T. Yang, 1987, "gas separation by adsroption processes", Butterworth, Boston.

[17] Hayashi, S., Kawai, M., and Kaneko, T., 1996, "Dynamics of High Purity Oxygen PSA", Gas Separation & Purification, 10(1) pp. 19-23.

[18] Maroulis, P. J., and Coe, C. G., 1989, "Calcium Chabazite Adsorbent for the Gas Chromatographic Separation of Trace Argon-Oxygen Mixtures", Analytical Chemistry, 61(10) pp. 1112-1117.

[19] K.S. Knaebel, A. K., 1993, "Pressure Swing Adsorption System to Purify Oxygen", 859227(US Patent 5,226,933).

[20] Sebastian, J., and Jasra, R. V., 2003, "Anomalous Adsorption of Nitrogen and Argon in Silver Exchanged Zeolite A", Chemical Communications, (2) pp. 268-269.

[21] Anson, A., Kuznicki, S. M., Kuznicki, T., 2009, "Separation of Argon and Oxygen by Adsorption on a Titanosilicate Molecular Sieve", Separation Science and Technology, 44(7) pp. 1604-1620.

[22] Hutson, N. D., Reisner, B. A., Yang, R. T., 2000, "Silver Ion-Exchanged Zeolites Y, X, and Low-Silica X: Observations of Thermally Induced Cation/Cluster Migration and the Resulting Effects on the Equilibrium Adsorption of Nitrogen", Chemistry of Materials, 12(10) pp. 3020-3031.

[23] Ansón, A., Kuznicki, S. M., Kuznicki, T., 2008, "Adsorption of Argon, Oxygen, and Nitrogen on Silver Exchanged ETS-10 Molecular Sieve", Microporous and Mesoporous Materials, 109(1-3) pp. 577-580.

[24] Kuznicki, and S. M., 1991, "Large-Pored Crystalline Titanium Molecular Sieve Zeolites", 07/348,226(US Patent 5011591) .

[25] Kuznicki, S. M., Bell, V. A., Nair, S., 2001, "A Titanosilicate Molecular Sieve with Adjustable Pores for Size-Selective Adsorption of Molecules", Nature, 412(6848) pp. 720-724.

[26] Kuznicki, S. M., Anson, A., Koenig, A., 2007, "Xenon Adsorption on Modified ETS-10", The Journal of Physical Chemistry C, 111(4) pp. 1560-1562.

[27] Sun, T., and Seff, K., 1994, "Silver Clusters and Chemistry in Zeolites", Chemical Reviews, 94(4) pp. 857-870.

Chapter 5

The Effect of Mixed Cation Exchange on Adsorption Properties of ETS–10

5.1 Introduction

Molecular sieves such as zeolites and mixed coordination materials carry a large extent of exchangeable cations in their structures to preserve the molecular sieve's neutrality. These extra-framework cations present in the molecular sieves structure as active sites in adsorption play a very substantial role in adjusting the adsorptive properties and changing the adsorbate-adsorbent interaction. Therefore, adsorption capacity, selectivity, and heat of adsorption are highly dependent upon density and localization of the cations in the molecular sieve structure [1-4]. Cation substitution may effectively result in changing the pore sizes (bigger or smaller) by either diminishing the number of cations present in the zeolite structure or relocating the cations but it is just limited to some certain structure [2, 3, 5]. For instance, by substituting sodium with potassium in zeolite NaA, effective pore size reduces from 3.8 Å to 3.3 Å since potassium with larger cationic diameter (2.66 Å) comparing to that of sodium (1.90 Å) blocks pore

openings of the zeolite A to some extent. This pore size reduction doesn't occur constantly with increasing ion exchange but it changes as it reaches 25% of potassium (based on cation exchange capacity). In a similar way, by calcium exchanging of NaA, pore size will sharply increase to 4.3 Å after 30% exchange since two Na^+ are replaced with one Ca^{2+}. While similar trends have been seen for zeolite chabazite, zeolite X shows a slight reduction in the pore size as it is exchanged with calcium exchange [2].

Based on the zeolite structure, high proportion of extra-framework cations is in contact with adsorbates which are small enough to go into the crystalline structure of the zeolite. Polar and polarizable adsorbates could interact strongly with these cations and adsorb selectively from a mixture of less polar or polarizable species [3]. N_2 has a bigger quadrupole moment (0.31 $Å^3$) than that of O_2 (0.1 $Å^3$) and therefore it adsorbs more strongly to the cationic sites than O_2 and it is much more sensitive to the charge density of the cation present. From the thermodynamic point of view, the zeolite is preferential to more strongly adsorbed species. In other words, N_2 interaction energy and adsorptive properties are more dependent on the choice of exchangeable cations present in the framework than that of O_2 with smaller quadrupole moment [3, 6-10]. Adsorption of N_2 and O_2 on different types of zeolites such as chabazite, mordenite, A, and X exchanged with different alkali and alkaline earth metal cations has been studies comprehensively and the influences of different cations are quantitatively understood [1, 3, 4, 7, 11-15]. It is demonstrated that zeolite chabazite is a good adsorbent to separate N_2 from O_2 and Ar. Singh et al. measured adsorption capacity and selectivity of N_2, O_2, and Ar on Na-Chabazite, K-Chabazite and Ca-chabazite at 273 K and 1 bar and observed that although Ca-chabazite showed higher selectivity for N_2/O_2 and higher adsorption capacity for N_2. However, higher O_2/Ar selectivity obtained using K-chabazite which was probably as a result of partial pore blockage owing to larger potassium cations [1]. Ca-chabazite is known as a practical gas chromatographic packing for separation and analyzing N_2 and some other gases including H_2, Ar, O_2, CH_4 and CO [9]. While zeolite LiX in which 86 equivalent percent or less of the cations are Li in balance with Na cations has been proposed

to improve adsorption capacity and also selectivity of N_2 significantly from a mixture of less polar or less polarizable adsorbates. This is a good choice of adsorbent for PSA units for N_2 purification [13]. A binary zeolite Ca/SrX with 5% to 40% Ca^{2+} balanced with Sr^{2+} was introduced as a useful adsorbent for adsorption of N_2 from air at super-ambient pressures to produce O_2 rich product stream [16]. Among monovalent alkali metal cation-exchanged zeolite X, the following trend of $Li^+>Na^+>K^+>Cs^+$ has been observed for N_2 adsorption capacity and N_2/O_2 selectivity. The highest adsorption properties was obtained for LiX which is probably due to bigger quadrupole of N_2 and concomitantly stronger interaction with Li^+ with its higher charge density compared to other members of the same group [4, 11]. Unlike the alkali cation-exchanged zeolite X, the reverse trend has seen when zeolite X was exchanged with divalent alkali earth metal cations: $Ba^{2+}>Sr^{2+}>Ca^{2+}>Mg^{2+}$ [7]. According to Coe et al., polyvalent-exchanged forms of zeolite faujasite (with Si/Al ratio of 1 to 2) particularly Mg^{2+}, Ca^{2+}, Sr^{2+}, and Ba^{2+} cation forms are proposed as superior adsorbents rather than monovalent-exchanged forms for separating N_2 from air [3]. Some research approaches are directed towards enhancing the effect of one cation in combination with other cations [12, 17, 18]. It has been reported that adsorptive properties of zeolite LiX and zeolite LiA would be improved significantly if a combination of Li^+ with alkaline-earth metal cations [17] and trivalent cations such as Al^{3+}, La^{3+}, Ce^{3+} [18] with several specific molar ratios is used as extra-framework cations instead of only Li^+ in N_2 separation from air by PSA.

Separation of Ar and O_2 is very challenging owing to their similar physical properties such as kinetic diameters, boiling points, polarizability of Ar atoms and O_2 molecules and consequently their adsorption behavior. Exploiting cryogenic distillation or pressure swing adsorption units for atmospheric air separation, O_2 product stream with concentration of 95% O_2 and 5% Ar could be obtained. Although this purity of O_2 is appropriate for most industrial applications, still higher purity of O_2 is required for some applications such as plasma chemistry, Ozone generator, and medical purposes [19]. In addition, Ar recovery with high purity is significantly needed for applications such as welding, electrical

appliances, and degassing in steel production. It is worth to mention that due to very small amount of Ar in O_2, the best adsorbent for this purpose must be selective towards Ar [20]. Numerous attempts have been made to develop an adsorbent which can selectively adsorb one of the Ar or O_2 in the mixture. It has been suggested that by using carbon molecular sieves (CMS), high purity of Ar could be obtained based on kinetically adsorption of O_2 rather than Ar owing to smaller kinetic diameter of O_2 comparing to Ar [20-23]. For instance, Miller et al. suggested that a two-bed PSA unit with CMS adsorbent could be utilized to gain a very high pure O_2 product with purity up to 99.6% from a mixture 95% O_2 and 5% Ar. This increase in O_2 purity is due to its selectively adsorption on the adsorbent [23]. Having measured equilibrium adsorption isotherms and capacity of Ar and O_2 on Na, Ca, Sr, and Ba–exchanged zeolite X at 288 K and 303 K, it was observed that adsorption capacity and O_2/Ar selectivity of alkaline-earth cation exchanged zeolite X were higher than that of NaX. While among these divalent exchanged forms, SrX had the highest O_2/Ar selectivity, the highest adsorption capacity belonged to CaX [24]. In the similar work, adsorption of N_2, O_2, and Ar on La^{3+}, Ce^{3+}, alkaline metals, and alkaline-earth metals cation-exchanged zeolite mordenite with Si/Al = 5.5 has been studied and the highly dependence of adsorption capacity, selectivity and heat of adsorption on the type, quantity, and the location of the extra-framework cations was observed. It was shown that the highest Ar and O_2 capacity, N_2 capacity and N_2/O_2 and O_2/Ar selectivity belonged to Ba–, Li– and Sr–mordenite, respectively [25].

It is believed that silver as an extra–framework cation can significantly enhance adsorption properties in molecular sieves which can be explained based on π–complexation theory described by Dewar in 1951 [26] and unique capability of d–orbitals in silver. It has been reported that mixed Li_xAg_y–zeolite X with just small amount of silver exhibits a considerably higher N_2/O_2, O_2/Ar selectivities and capacities than those of Li–X [8, 18, 26-29]. Sebastian et al. compared adsorption characteristics of Ag–A with Na–A and Ca–A at two different pressures of 6.66 kPa and 101.99 kPa and concluded that Ag–A has the highest amounts of heat of adsorption, capacities, and N_2/O_2 and Ar/O_2 selectivities. The

adsorption selectivity and capacity are substantially key parameters to determine the size of the adsorber. The higher the selectivity and capacity, the lower the cost of oxygen and Nitrogen production would be [30, 31]. Studying the adsorption of Ar, N_2, and O_2 on various sodium– and silver–exchanged forms of zeolites including zeolites A, X, Y, Mordenite, ZSM–5, and BEA shows that silver–exchanged types in all zeolites have the higher capacities of all three adsorbates as well as higher selectivities of N_2/O_2 and Ar/O_2 which make them potential adsorbents for oxygen production with high purity. On the other hand, among the silver–exchanged zeolites, the highest amount of N_2/O_2 and Ar/O_2 selectivities at 101.99 kPa and 288.2 K belonged to zeolite A and zeolite ZSM–5, respectively [32].

In this work, ETS–10 molecular sieve has been synthesized and exchanged with alkaline and alkaline earth metal cations, such as Li^+, K^+, Na^+, Mg^{2+}, Ca^{2+}, Sr^{2+}, and Ba^{2+} and then their mixed exchanged with silver is prepared. The objective is to understand the effect of these cations and their combinations with silver on the adsorption capacity and selectivity of nitrogen, argon, and oxygen.

5.2 Experimental Methods

Materials. ETS–10 was synthesized hydrothermally according to the procedure reported by Kuznicki as explained before [33]. Other salts required for ion exchange including: LiCl, KCl, $BaCl_2$, $SrCl_2$, $CaCl_2$, $MgCl_2$, and $AgNO_3$, were obtained from Fisher.

Single Cation Exchange. In order to prepare various cation–exchanged forms of ETS–10, as–synthesized ETS–10 powder was exposed to an 3–fold excess amount of aqueous solution of different salts (i.e. LiCl, $BaCl_2$, $SrCl_2$,…) at 353 K overnight. This process was repeated three to four times consecutively to ensure that it is mostly exchanged. The exchanged materials were thoroughly washed and vacuum filtered with sufficient amount of de–ionized water after each exchange and finally dried in the oven at 353 K. Since as–synthesized ETS–10 was sodium and potassium based, in all cases small amount of Na^+ and K^+ was present.

Mixed Cation Exchange with silver. Mixed cationic forms of ETS–10 were made by exposing "single cation-exchanged samples" to an aqueous solution of $AgNO_3$. Since the silver cations can simply and quickly exchange, one time silver exchange is done. To prepare two series of samples with two different levels of silver, the amount of silver introduced to the exchanged–solution was: half and one–third of the ETS–10 original cation–exchange capacity (CEC = 5), respectively.

5.3 Results and Discussion

X–ray powder diffraction (XRD) and scanning electron microscopy (SEM) analyses were done as explained in the chapter 4. The XRD patterns of all cation–exchanged samples shown in Figure (5.1) confirmed that the crystalline structure of ETS–10 samples was retained after several consecutive cation exchanges because the X–ray diffraction patterns of the samples showed the typical peaks of ETS–10.

Images collected form SEM also verified that the original cubic well–defined crystalline structure of all exchanged samples was intact during ion exchange and the cation–exchange modifications was observed on the cubic surfaces.

Table (5.1) reports the equilibrium adsorption capacities of different cation–exchanged ETS–10 at 298 K and atmospheric pressure calculated from adsorption isotherms. It is clear that Li–ETS–10 has the highest adsorption capacity for nitrogen compared to others given in Table (5.1) and then Ba– and Sr–ETS–10 come to the second and third place. In various research attempts on other zeolites such as zeolite X and mordenite, it is shown that the highest N_2 capacity belongs to Li–exchanged zeolite. This is probably owing to bigger quadrupole of N_2 and consequently stronger interaction with Li^+ [4, 7, 13, 25]. It is also suggested that N_2 adsorption capacity of alkali metal exchanged–zeolite X is following the order of $Ba^{2+}>Sr^{2+}>Ca^{2+}>Mg^{2+}$ [7] as seen in ETS–10. The highest capacities for Ar and O_2 also belong to Li–ETS–10 and Sr–ETS–10, respectively.
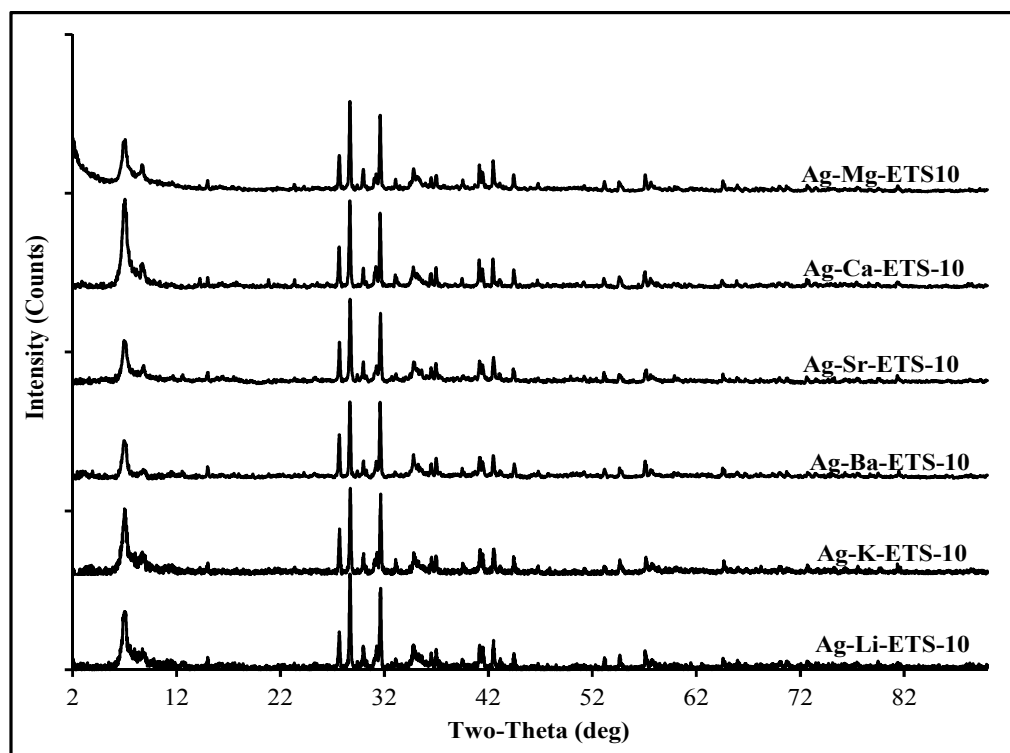
Figure 5.1 XRD patterns for various cation–exchanged ETS–10

Different cation–exchanged forms of ETS–10 show much higher Ar, O_2, and N_2 capacities than those of other zeolites such as mordenite, zeolite X, and A.

Table 5.1 Nitrogen, oxygen, and argon Langmuir parameters (q_m) on various cation–exchanged ETS–10 at 298 K and 1 atm

Adsorbent	Nitrogen	Oxygen	Argon
Li–ETS–10	27.61	39.13	50.65
Sr–ETS–10	21.01	62.79	48.65
Ba–ETS–10	22.95	41.44	33.44
Ag–Li–ETS–10	14.13	29.63	24.00
Ag–K–ETS–10	14.75	33.29	27.81
Ag–Ca–ETS–10	15.58	34.16	26.52
Ag–Ba–ETS–10	14.99	26.47	23.04

Henry's constants and the selectivity of nitrogen/oxygen and argon/oxygen on several cation-exchanged ETS–10 samples are given in Tables (5.2) and (5.3), respectively. These values are calculated from equilibrium adsorption isotherms at 298 K and 1 atm.

Table 5.2 Henry's constant for nitrogen, oxygen, and argon on different cation–exchanged ETS–10 at 298 K and 1 atm

Adsorbent	Henry's Constant, K (mmol kPa^{-1} g^{-1}) at 298 K		
	N_2	O_2	Ar
Li–ETS–10	0.0050	0.0022	0.0022
Sr–ETS–10	0.0039	0.0017	0.0018
Ba–ETS–10	0.0028	0.0016	0.0017
Ag–ETS–10	0.0287	0.0022	0.0031
Ag–Li–ETS–10	0.0229	0.0026	0.0033
Ag–K–ETS–10	0.0177	0.0024	0.0032
Ag–Ca–ETS–10	0.0269	0.0031	0.0040
Ag–Ba–ETS–10	0.0256	0.0026	0.0035

Table 5.3 N_2/O_2 and Ar/O_2 selectivities on various cation–exchanged ETS–10 at 298 K and 1 atm obtained from equilibrium isotherms

Adsorbent	Equilibrium Adsorption Selectivity at Henry's region		
	N_2/O_2	N_2/Ar	Ar/O_2
Li–ETS–10	2.27	2.27	1.00
Sr–ETS–10	2.32	2.17	1.07
Ba–ETS–10	1.77	1.65	1.08
Ag–ETS–10	13.05	9.26	1.41
Ag–Li–ETS–10	8.81	6.94	1.27
Ag–K–ETS–10	7.38	5.53	1.33
Ag–Ca–ETS–10	8.68	6.73	1.29
Ag–Ba–ETS–10	9.14	7.31	1.35

According to the data given in Table (5.2), as silver is added to the ETS–10 structure the amount of Henry's constants jump comparing to the single cation–exchanged ETS–10. Ag–Ca–ETS–10 has the highest values for the N_2, O_2, and Ar Henry's constants and Ag–Ba–ETS–10 comes in the second place. Single cation–exchanged–ETS–10 molecular sieves exhibit some acceptable level of N_2/O_2 and N_2/Ar selectivities, while their selectivity for Ar/O_2 is too low, shown in Table (5.3). When it comes to mixed–exchanged ETS–10, selectivities have increased significantly. This reveals how incorporation of only small amount of silver which is half the cation exchange capacity of ETS–10 enhances adsorptive properties and selectivities especially Ar/O_2 selectivity. For instance, in the case of Li–ETS–10, after introduction silver, the N_2/O_2 selectivity has increased by 6.54 and the Ar/O_2 selectivity is improved from non-selective Li–ETS–10 to Ar selective Ag–Li–ETS–10 with value of 1.27. Based on the adsorption equilibrium isotherms, Ag–Ba–ETS–10 has the highest N_2/O_2, N_2/Ar, and Ar/O_2 selectivites among others.

Sebastian et al. compared a wide range of fully silver exchanged zeolite A, X, Y, mordenite, ZSM–5, and BEA by other cationic exchange forms and concluded that introduction of silver to the crystalline structure of zeolite significantly improves the adsorptive properties such as selectivities and capacities [32]. The amount of N_2/O_2 selectivities of mixed silver exchanged ETS–10 with only a little amount of silver are much higher than those reported by [32] at the same condition not to mention higher or comparable Ar/O_2 selectivity.

The equilibrium adsorption selectivities for nitrogen over oxygen and argon over oxygen at atmospheric pressure and 303 K obtaining from inverse gas chromatography are given in Table (5.4). IGC was performed at 303 K, while the isotherms were collected at 298 K.

Table 5.4 N_2/O_2 and Ar/O_2 selectivities on various cation–exchanged ETS–10 at 303 K and 1 atm obtained from IGC

Adsorbent	Equilibrium Adsorption Selectivity	
	N_2/O_2	Ar/O_2
Li–ETS–10	2.47	1.01
Na–ETS–10	2.89	1.01
K–ETS–10	2.19	1.02
Mg–ETS–10	1.56	1.04
Ca–ETS–10	2.11	1.02
Sr–ETS–10	2.33	1.01
Ba–ETS–10	1.92	1.01
Ag–ETS–10	11.5	1.4
Ag–Li–ETS–10	7.44	1.24
Ag–Na–ETS–10	8.96	1.25
Ag–K–ETS–10	8.03	1.24
Ag–Mg–ETS–10	10.17	1.30
Ag–Ca–ETS–10	10.23	1.30
Ag–Sr–ETS–10	9.08	1.28
Ag–Ba–ETS–10	9.89	1.32
Ag/3–Mg–ETS–10	4.81	1.17
Ag/3–Ca–ETS–10	7.53	1.23
Ag/3–Sr–ETS–10	5.61	1.16
Ag/3–Ba–ETS–10	7.68	1.24

Single alkaline and alkaline earth metal cation–exchanged ETS–10 plus mixed–exchanged ETS–10 with introduction of half and one–third of CEC of silver are tested on IGC. The main purpose of preparing samples with two different amounts of silver is to investigate the influence of the silver level in the selectivities.

As reported in Table (5.4), after full silver exchanged ETS–10, mixed silver–divalent cation exchanged ETS–10 adsorbents have the highest N_2/O_2 and Ar/O_2 selectivities and among them Ag–Ba and Ag–Ca show the maximum Ar/O_2 and N_2/O_2 selectivity, respectively. Comparing mixed silver–divalent cation exchanged samples, as the level of the silver drops from CEC/2 to CEC/3, selectivites decreases a little bit and the highest selectivities goes for Ag/3–Ba and then Ag/3–Ca. Among mixed silver–monovalent cation exchanged ETS–10 samples, Ag–Na has the maximum N_2/O_2 and Ar/O_2 selectivity. While Ag–Li and Ag–K both have the same amount of Ar/O_2 selectivity, Ag–K exhibits higher N_2/O_2 selectivity than that of Ag–Li. Although mixed silver–monovalent cation exchanged samples have higher amount of silver than those mixed silver–divalent cation exchanged samples by CEC/3 silver, their selectivities is very close. In the case of single exchanged samples, they all show N_2/O_2 selectivity to some extent while their Ar/O_2 selectivity is too low.

Figure (5.2) demonstrates IGC profiles for Ag–Na–ETS–10, Ag–Ba–ETS–10, and Ag/3–Ba–ETS–10 chosen as candidates. In each case, pure Ar and O_2, 50–50% mixture Ar/O_2, and Air are injected. In all profiles, the retention times for pure argon are larger than pure oxygen which is indicating an affinity for argon over oxygen in silver–exchanged ETS–10. As shown in the IGC plots, chromatographic splitting for mixed Ar/O_2 injection is much more obvious on Ag–Ba–ETS–10 adsorbent compared to Ag–Na–ETS–10 and Ag/3–Ba–ETS–10. This also can be verified from the selectivities obtained from IGC.

Figure (5.3) shows nitrogen, argon, and oxygen adsorption isotherms on several of the cation–exchanged ETS–10 samples with their Langmuir fitting curves up to a pressure of 120 kPa. As seen in the Figure (5.3), adsorption isotherms of Ba– and Sr–ETS–10 are linear and as silver is introduced to their structures, the isotherm changes to rectangular shape especially N_2 isotherm owing to bigger quadrupole moment of N_2. Sharp increase in the adsorptive capacities is obvious as well.
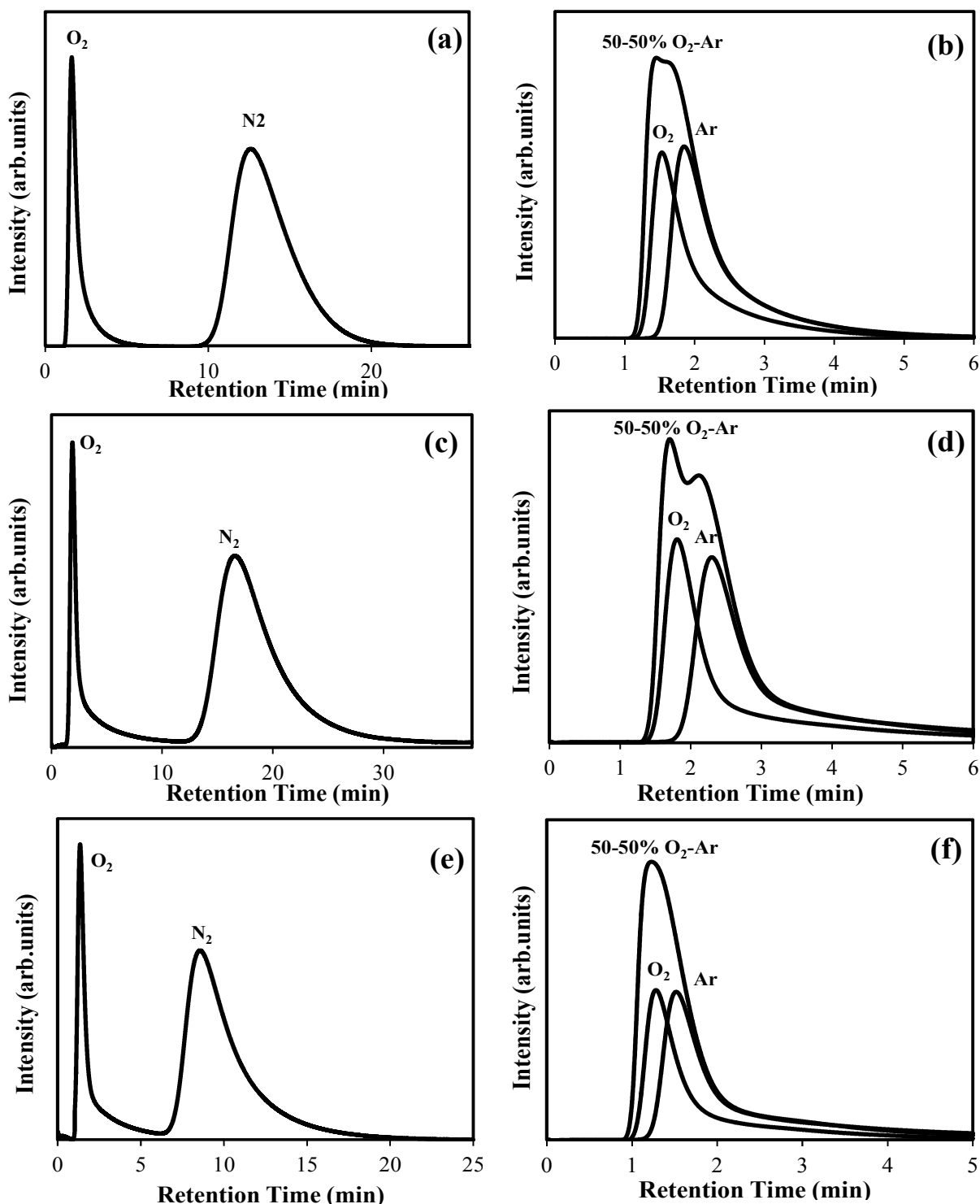
Figure 5.2 IGC profiles obtained at 303 K with 30 ml/min helium carrier gas for Ar, O_2, a 50–50% mixture of Ar/O_2, and Air on (a,b) Ag–Na–ETS–10, (c,d) Ag–Ba–ETS–10, and (e,f) Ag/3–Ba–ETS–10
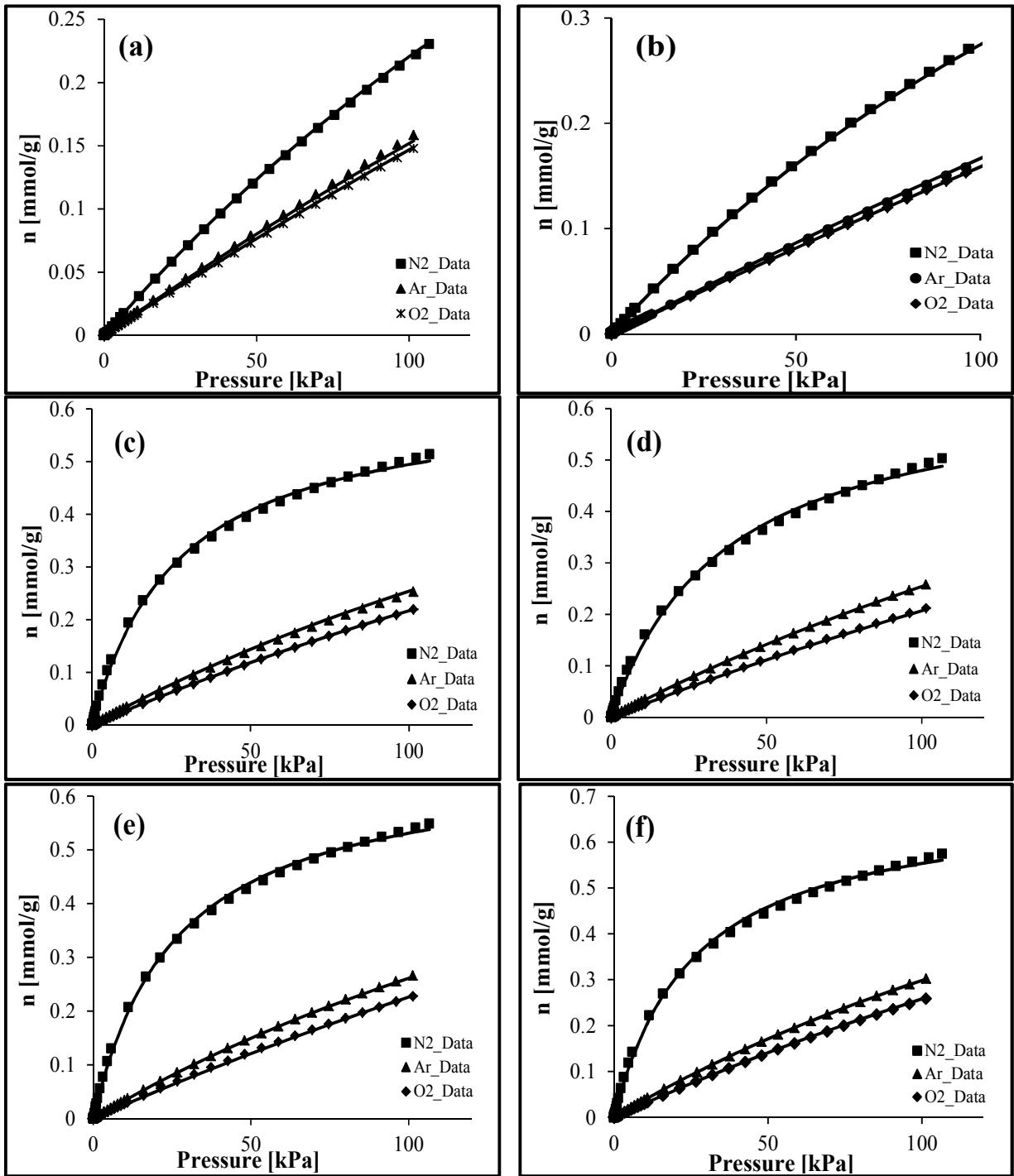
Figure 5.3 Nitrogen, argon, and oxygen adsorption isotherms at 298 K on (a) Ba–ETS–10, (b) Sr–ETS–10, (c) Ag–Li–ETS–10, (d) Ag–K–ETS–10, (e) Ag–Ba–ETS–10, and (f) Ag–Ca–ETS–10

5.5 Conclusions

Adsorption of nitrogen, oxygen, and argon on several single and mixed cation–exchanged ETS–10 molecular sieves was studied at atmospheric pressure and temperature of 303K for IGC and 298K for adsorption isotherm data.

Unlike other cation-exchanged ETS–10 adsorbents that show very small Ar/O_2 selectivity, mixed silver-exchanged ETS–10 adsorbents exhibit some reasonable extent of Ar/O_2 selectivity and significantly high N_2/O_2 selectivity. This shows how introduction of only small amount of silver to the ETS–10 crystalline structure improves its adsorptive properties. Combining different cations with silver has different effects in the adsorptive properties of ETS–10. It has been shown that Ag–Ba–ETS–10 has the highest Ar/O_2 selectivity while the maximum N_2/O_2 selectivity belongs to Ag–Ca–ETS–10. On the other hand, the values obtained for selectivities are bigger in mixed silver–divalent cation exchanged ETS–10 samples than those of mixed silver–monovalent cation exchanged samples.

As the amount of silver introduced has been decreased to one–third of CEC of ETS–10 in mixed silver–divalent cation exchanged ETS–10 adsorbents, still there are high selectivities for N_2/O_2 and Ar/O_2 which are comparable with the values obtained for mixed silver–monovalent ETS–10 with half CEC of silver. Due to the high cost of silver salt this is a good method to take advantage of making a mixed combination of divalent alkaline earth metal cations and silver in ETS–10 structure molecular sieves.

References:

[1] Singh, R. K., and Webley, P., 2005, "Adsorption of N_2, O_2, and Ar in Potassium Chabazite", Adsorption, 11(0) pp. 173-177.

[2] Breck, D.W., 1974, "Zeolite molecular sieves: structure, chemistry, and use", Wiley, New York.

[3] Charles, G. C., and Steven M., K., 1984, "Polyvalent Ion Exchanged Adsorbent Fro Air Separation", 441,822 (US Patent 4,481,018).

[4] Jasra, R. V., Choudary, N. V., and Bhat, S. G. T., 1996, "Correlation of Sorption Behavior of Nitrogen, Oxygen, and Argon with Cation Locations in Zeolite X", Industrial & Engineering Chemistry Research, 35(11) pp. 4221-4229.

[5] Lin, C. C. H., Sawada, J. A., Wu, L., 2009, "Anion-Controlled Pore Size of Titanium Silicate Molecular Sieves", Journal of the American Chemical Society, 131(2) pp. 609-614.

[6] Häring, H., February 2008, "Industrial Gases Processing", Wiley-VCH, Weinheim Germany.

[7] Douglas W., M., 1964, "Separation of an Oxygen-Nitrogen Mixture", 73,215 (US Patent 3140932).

[8] Hutson, N. D., Rege, S. U., and Yang, R. T., 1999, "Mixed Cation Zeolites: Li_xAg_y-X as a Superior Adsorbent for Air Separation", AICHE Journal, 45(4) pp. 724-734.

[9] Maroulis, P. J., and Coe, C. G., 1989, "Calcium Chabazite Adsorbent for the Gas Chromatographic Separation of Trace Argon-Oxygen Mixtures", Analytical Chemistry, 61(10) pp. 1112-1117.

[10] Baksh, M. S. A., Kikkinides, E. S., and Yang, R. T., 1992, "Lithium Type X Zeolite as a Superior Sorbent for Air Separation", Separation Science and Technology, 27(3) pp. 277-294.

[11] Douglas W., M., 1964, "Separation of an Oxygen-Nitrogen Mixture", 73,216 (US Patent 3140933).

[12] H. W. Habgood, 1964, "Adsorptive and Gas Chromatographic Properties of Various Cationic Forms of Zeolite X", Canadian Journal of Chemistry, 42pp. 2340.

[13] Chien C., C., and Millwood, N. Y., 1989, "Process for Separating Nitrogen from Mixtures Thereof with Less Polar Substances", 67820 (US Patent 4859217) .

[14] Da-Ming, S., 1991, "The Effect of Ion Exchange on Adsorption Properties of a 13X Molecular Sieve", Vacuum, 42(13) pp. 845-848.

[15] Furuyama, S., and Nagato, M., 1984, "Sorption of Argon, Oxygen, Nitrogen, Nitric Oxide, and Carbon Monoxide by Magnesium, Calcium, and Barium Mordenites", The Journal of Physical Chemistry, 88(9) pp. 1735-1740.

[16] S., S., R.R., C., and W. J., A., 1985, "Binary Ion Exchanged Type X Zeolite Adsorbent", 665794 (US Patent 4557736).

[17] Chien C., C., John D., S., Joseph T., M., 1995, "Mixed Ion-Exchanged Zeolites and Processes for the use Thereof in Gas Separations", 992187 (US Patent 5413625).

[18] Frank R., F., Martin, B., and Adeola F., O., 1995, "Adsorptive Separation of Nitrogen from Other Gases", 287324 (US Patent 5464467).

[19] Jayaraman, A., Yang, R. T., Cho, S., 2002, "Adsorption of Nitrogen, Oxygen and Argon on Na-CeX Zeolites", Adsorption, 8(4) pp. 271-278.

[20] Rege, S. U., and Yang, R. T., 2000, "Kinetic Separation of Oxygen and Argon using Molecular Sieve Carbon", Adsorption, 6(1) pp. 15-22.

[21] Jin, X., Malek, A., and Farooq, S., 2006, "Production of Argon from an Oxygen'Argon Mixture by Pressure Swing Adsorption", Industrial & Engineering Chemistry Research, 45(16) pp. 5775-5787.

[22] Baksh, M. S. A., and Stewart, A. B., 2003, "Argon Purification Process", 09750085 (US Patent 6527831).

[23] Miller, G. W., and Theis, C. F., 1989, "Secondary Oxygen Purifier for Molecular Sieve Oxygen Concentrator", 07151383 (US Patent 4813979).

[24] Peter, S. A., Moharir, A. S., and Jasra, R. V., 2010, "Selective Adsorption of Oxygen Over Argon in Alkaline-Earth-Metal Cation-Exchanged Zeolite X", Industrial & Engineering Chemistry Research, 49(16) pp. 7524-7529.

[25] Peter, S. A., Sebastian, J., and Jasra, R. V., 2005, "Adsorption of Nitrogen, Oxygen, and Argon in Mono-, Di-, and Trivalent Cation-Exchanged Zeolite Mordenite", Industrial & Engineering Chemistry Research, 44(17) pp. 6856-6864.

[26] Yang, R. T., Chen, Y. D., Peck, J. D., 1996, "Zeolites Containing Mixed Cations for Air Separation by Weak Chemisorption-Assisted Adsorption", Industrial & Engineering Chemistry Research, 35(9) pp. 3093-3099.

[27] Hutson, N. D., and Yang, R. T., 2000, "Structural Effects on Adsorption of Atmospheric Gases in Mixed Li,Ag-*X*-Zeolite", AICHE Journal, 46(11) pp. 2305-2317.

[28] Yang, R. T., and Hutson, N. D., 2004, "Lithium-Based Zeolites Containing Silver and Copper and use Thereof for Selective Adsorption", 09/869623 (US Patent 6780806).

[29] Chiang, R. L., Whitley, R. D., Ostroski, J. E., 2002, "Argon/Oxygen Selective X-Zeolite", 09/782265 (US Patent 20020108495) .

[30] Sebastian, J., and Jasra, R. V., 2003, "Anomalous Adsorption of Nitrogen and Argon in Silver Exchanged Zeolite A", Chemical Communications, (2) pp. 268-269.

[31] Sebastian, J., and Jasra, R. V., 2003, "Process for the Preparation of Molecular Sieve Adsorbent for Selective Adsorption of Nitrogen and Argon", 10/105876 (US Patent 6572838 B1).

[32] Sebastian, J., and Jasra, R. V., 2005, "Sorption of Nitrogen, Oxygen, and Argon in Silver-Exchanged Zeolites", Industrial & Engineering Chemistry Research, 44(21) pp. 8014-8024.

[33] Kuznicki, and S. M., 1991, "Large-Pored Crystalline Titanium Molecular Sieve Zeolites", 07/348,226 (US Patent 5011591).